Published for SISSA by Springer

Received: April 13, 2022
Revised: July 5, 2022
Accepted: July 21, 2022
Published: August 19, 2022

Mounting evidence for a 95 GeV Higgs boson

T. Biekötter,[a] **S. Heinemeyer**[b] **and G. Weiglein**[a,c]

[a] *Deutsches Elektronen-Synchrotron DESY, Notkestr. 85, 22607 Hamburg, Germany*

[b] *Instituto de Física Teórica UAM-CSIC, Universidad Autónoma de Madrid, Cantoblanco, 28049, Madrid, Spain*

[c] *II. Institut für Theoretische Physik, Universität Hamburg, Luruper Chaussee 149, 22761 Hamburg, Germany*

E-mail: thomas.biekoetter@desy.de, Sven.Heinemeyer@cern.ch, georg.weiglein@desy.de

Abstract: In 2018 CMS reported an excess in the light Higgs-boson search in the diphoton decay mode at about 95 GeV based on Run 1 and first year Run 2 data. The combined local significance of the excess was $2.8\,\sigma$. The excess is compatible with the limits obtained in the ATLAS searches from the diphoton search channel. Recently, CMS reported another local excess with a significance of $3.1\,\sigma$ in the light Higgs-boson search in the di-tau final state, which is compatible with the interpretation of a Higgs boson with a mass of about 95 GeV. We show that the observed results can be interpreted as manifestations of a Higgs boson in the Two-Higgs Doublet Model with an additional real singlet (N2HDM). We find that the lightest Higgs boson of the N2HDM can fit both excesses simultaneously, while the second-lightest state is such that it satisfies the Higgs-boson measurements at 125 GeV, and the full Higgs-boson sector is compatible with all Higgs exclusion bounds from the searches at LEP, the Tevatron and the LHC as well as with other theoretical and experimental constraints. Finally, we demonstrate that it is furthermore possible to accommodate the excesses observed by CMS in the two search channels together with a local $2.3\,\sigma$ excess in the $b\bar{b}$ final state observed at LEP in the same mass range.

Keywords: Multi-Higgs Models, Specific BSM Phenomenology

ArXiv ePrint: 2203.13180

https://doi.org/10.1007/JHEP08(2022)201

JHEP08(2022)201

Contents

JHEP08(2022)201

1 Introduction

In the year 2012 the ATLAS and CMS collaborations discovered a new particle [1–3] that — within the present theoretical and experimental uncertainties — is consistent with the predictions for the Higgs boson of the Standard Model (SM) at a mass of about 125 GeV, but is also compatible with the predictions of a wide variety of extensions of the SM. While no conclusive signs of physics beyond the SM (BSM) have been found so far at the LHC, both the measurements of the properties of the discovered state at 125 GeV (its couplings are known up to now to an experimental precision of roughly 20%) and the existing limits from the searches for new particles leave significant room for interpretations in models of physics beyond the SM. Many BSM models feature extended Higgs-boson sectors. Consequently, one of the main tasks of the LHC Run 3 and beyond will be to determine whether the observed scalar boson forms part of the Higgs sector of an extended model. Extended Higgs-boson sectors naturally contain additional Higgs bosons with masses larger than 125 GeV. However, many extensions also offer the possibilty of additional Higgs bosons that are *lighter* than 125 GeV. Accordingly, the search for light additional Higgs bosons is of crucial importance for exploring the underlying physics of electroweak symmetry breaking.

Searches for Higgs bosons below 125 GeV have been performed at LEP [4–6], the Tevatron [7] and the LHC [8–12]. Results based on the first year of CMS Run 2 data for Higgs-boson searches in the diphoton final state show a local excess of about $3\,\sigma$ at a mass of 95 GeV [9], which received considerable attention also in view of the fact that a similar excess of $2\,\sigma$ occurred in the Run 1 data at a comparable mass [13]. Combining 7, 8 and first year 13 TeV data (and assuming that the gg production dominates) the excess is most

pronounced at a mass of 95.3 with a local significance of $2.8\,\sigma$. From the excess of events CMS obtained a signal strength of

$$\mu_{\gamma\gamma}^{\text{exp}} = \frac{\sigma^{\text{exp}}\,(gg \to \phi \to \gamma\gamma)}{\sigma^{\text{SM}}\,(gg \to H \to \gamma\gamma)} = 0.6 \pm 0.2\,. \tag{1.1}$$

Here the SM prediction, σ^{SM}, is evaluated for a SM Higgs-boson mass of 95.3 GeV. First Run 2 results from ATLAS with $80\,\text{fb}^{-1}$ in the $\gamma\gamma$ searches below 125 GeV were reported in 2018 [11]. No significant excess above the SM expectation was observed in the mass range between 65 and 110 GeV. However, the limit on cross section times branching ratio obtained in the diphoton final state by ATLAS is not only well above $\mu_{\gamma\gamma}^{\text{exp}}$, but even weaker than the corresponding upper limit obtained by CMS at and around 95 GeV. This was illustrated in figure 1 of ref. [14] (based on the Run 1 and first year Run 2 data).

Searches for a low-mass Higgs boson that were previously carried out at LEP resulted in a $2.3\,\sigma$ local excess observed in the $e^+e^- \to Z(H \to b\bar{b})$ searches [5] at a mass of about 98 GeV; due to the $b\bar{b}$ final state the mass resolution was rather coarse. The excess observed at LEP can be expressed in terms of a signal strength as

$$\mu_{bb}^{\text{exp}} = \frac{\sigma^{\text{exp}}\left(e^+e^- \to Z\phi \to Zb\bar{b}\right)}{\sigma^{\text{SM}}\left(e^+e^- \to ZH \to Zb\bar{b}\right)} = 0.117 \pm 0.057\,, \tag{1.2}$$

where in this case the observed cross section times branching ratio is normalized to the SM expectation for a SM Higgs boson with a mass of 98 GeV. The value for μ_{bb}^{exp} was extracted in ref. [15] using methods described in ref. [16]. It should be noted that μ_{bb}^{exp} was extracted at a slightly larger mass of 98 GeV compared to $\mu_{\gamma\gamma}^{\text{exp}}$ which was extracted assuming a mass of 95.3 GeV. However, because of the limited mass resolution in the $b\bar{b}$ final state at LEP the signal strength of the LEP excess extracted at 95 GeV is expected to be very close to the value μ_{bb}^{exp} as stated above, and we therefore use μ_{bb}^{exp} obtained at 98 GeV without modification.

Since the reported excesses in the $\gamma\gamma$ channel at the LHC and the $b\bar{b}$ channel at LEP were found at approximately the same mass, the question of a possible common origin received some attention in the literature. Specifically it was explored whether certain model realizations could simultaneously explain the two excesses, while being in agreement with all other Higgs-boson related limits and measurements. These possibilities were reviewed in refs. [14, 17, 18]. Models in which the two excesses can be described simultaneously comprise the extension by a Higgs singlet with additional vector-like matter [19], a radion model [20], type I 2HDMs with a moderately-to-strongly fermiophobic CP-even Higgs boson produced via decays of a charged Higgs boson lighter than the top quark [21], a minimal dilaton model [22], the $\mu\nu$SSM with one [23] and three generations [24] of right-handed neutrinos, a Higgs boson associated with the breakdown of an $\text{U}(1)_{L_\mu L_\tau}$ symmetry [25], a minimum stealth boson model [26], various realizations of the NMSSM [27, 28], including the inflation-inspired μNMSSM [29], and the NMSSM with a seesaw extension [30]. Furthermore, in ref. [31] the two excesses were studied in the 2HDM with an additional real singlet, the N2HDM [32, 33], with several follow-up analyses [34–38], where in ref. [38] also the

JHEP08(2022)201

2HDMS (the 2HDM plus a complex singlet and an additional Z_3 symmetry) was analyzed. In ref. [39] the possibility of a simultaneous description of the two excesses at 95 GeV and excesses reported by ATLAS and CMS near 400 GeV was investigated in the N2HDM and the NMSSM. In ref. [40] a complex singlet field instead of the real singlet field of the N2HDM was considered, and as a result also a valid dark-matter candidate can be present.

The analysis of ref. [31] in the context of the N2HDM revealed that only the so-called type II and type IV Yukawa structures can provide a description for the diphoton excess observed at CMS. Here a dominantly singlet-like Higgs boson with a mass of about 95 GeV acquires an enhancement of its branching ratio for the decay into $\gamma\gamma$ by means of a suppression of the partial decay width for the $b\bar{b}$ decay mode. While comparable values of $\mu_{\gamma\gamma}$ were shown to be realized in both the type II and type IV N2HDM, it was pointed out in ref. [31] that the type IV scenario also predicts sizable branching ratios of the state at 95 GeV decaying into pairs of τ-leptons. In contrast, the $\tau^+\tau^-$ decay mode is suppressed in type II in the parameter regions in which the $\gamma\gamma$-excess can be accommodated. As a consequence, the results for the low-mass Higgs-boson searches in the $\tau^+\tau^-$ final state are a crucial test for the N2HDM interpretation of the observed diphoton excess which can potentially discriminate between the type II and type IV scenarios.

In this context the recent results obtained by the CMS collaboration in the search for additional Higgs bosons in the $\tau^+\tau^-$ channel [12] are obviously of particular interest. Remarkably, utilizing the full Run 2 data set, in ref. [12] the CMS collaboration reported an excess in the low-mass region for the gluon-fusion production mode and subsequent decay into $\tau^+\tau^-$ pairs that is compatible with the excess that has been observed by CMS in the diphoton search (the latter search has not yet been updated to include the full Run 2 data). The excess in the $\tau^+\tau^-$ final state is most pronounced for a mass hypothesis of 100 GeV, with a local significance of $3.1\,\sigma$, while for a mass value of 95 GeV, i.e. close to the most significant excess in the $\gamma\gamma$ search [9], CMS reports a local significance of $2.6\,\sigma$. It should be noted in this context that up to now there exists no corresponding result for the low-mass search in the $\tau^+\tau^-$ final state from the ATLAS collaboration. For the CMS result, the best-fit cross section for a mass value of 95 GeV has been determined to be $\sigma_{gg\phi} \times \mathrm{BR}(\phi \to \tau^+\tau^-) = (7.7^{+3.9}_{-3.1})$ pb [12]. This corresponds to a signal strength of

$$\mu^{\mathrm{exp}}_{\tau\tau} = \frac{\sigma^{\mathrm{exp}}(gg \to \phi \to \tau^+\tau^-)}{\sigma^{\mathrm{SM}}(gg \to H \to \tau^+\tau^-)} = 1.2 \pm 0.5\,, \tag{1.3}$$

where we use a symmetric uncertainty interval for the signal strength that is obtained from the lower uncertainty interval of the quoted result for $\sigma_{gg\phi} \times \mathrm{BR}(\phi \to \tau^+\tau^-)$.[1]

The fact that the LHC searches for a low-mass Higgs boson have led to mutually compatible excesses in both investigated channels, $\gamma\gamma$ and $\tau^+\tau^-$, is a strong motivation for exploring a possible BSM nature of the observed patterns. In the present paper we will focus specifically on the interpretation in the context of the N2HDM, as motivated by the earlier analyses in refs. [31, 39]. Initially, we will investigate whether the N2HDM, depending on its Yukawa type, can simultaneously describe both the excesses in the $\gamma\gamma$

[1] The justification of this choice will be given in section 4.

JHEP08(2022)201

and $\tau^+\tau^-$ channels at the LHC. Subsequently, we then incorporate also the (statistically slightly less significant) $b\bar{b}$ excess observed at LEP into our analysis and investigate to what extent the observed patterns in all three search channels can be successfully described. We will moreover discuss the experimental prospects for further probing the possible presence of a new state at about 95 GeV in the near future.

The paper is organized as follows. After introducing the model in section 2 and the relevant theoretical and experimental constraints on the N2HDM parameter space in section 3, the numerical results of our parameter scan are presented in section 4, where also the future prospects are discussed. We summarize our results in section 5.

2 The N2HDM

The N2HDM is the simplest extension of a CP-conserving Two-Higgs doublet model (2HDM) in which the latter is augmented with a real scalar singlet Higgs field [32, 33]. After electroweak symmetry breaking, the fields can be parameterized as

$$\Phi_1 = \begin{pmatrix} \phi_1^+ \\ \frac{1}{\sqrt{2}}(v_1 + \rho_1 + i\eta_1) \end{pmatrix}, \quad \Phi_2 = \begin{pmatrix} \phi_2^+ \\ \frac{1}{\sqrt{2}}(v_2 + \rho_2 + i\eta_2) \end{pmatrix}, \quad \Phi_S = v_S + \rho_S\,, \tag{2.1}$$

where Φ_1 and Φ_2 are the two $\mathrm{SU}(2)_L$ doublets with hypercharge 1, and Φ_S is a real scalar singlet. The parameters v_1, v_2, v_S are the real vacuum expectation values (vevs) acquired by the fields Φ_1, Φ_2 and Φ_S, respectively. As in the 2HDM we define $\tan\beta := v_2/v_1$. A Z_2 symmetry is imposed on the scalar potential, which is only softly broken by a bilinear term usually written as $m_{12}^2(\Phi_1^\dagger\Phi_2 + \text{h.c.})$ (see, for instance, eq. (2.1) in ref. [33]). The Z_2 symmetry is extended to the Yukawa sector in order to eliminate tree-level flavor-changing neutral currents. As in the 2HDM, one can have four variants of the N2HDM, depending on the Z_2 parities of the fermions. We will focus on type II and IV (flipped), which were shown to be capable of accommodating the diphoton excess [31].[2] In addition, the scalar potential is invariant under a second Z_2 symmetry acting only on Φ_S. This symmetry is spontaneously broken if Φ_S acquires a vev.

In the CP-even scalar sector, the states ρ_1, ρ_2 and ρ_S mix, leading to a total of three CP-even physical Higgs bosons $h_{1,2,3}$, where we use the convention $m_{h_1} < m_{h_2} < m_{h_3}$. The relation between the two sets of states is given in terms of the 3×3 orthogonal matrix R, which can be parameterized as

$$R = \begin{pmatrix} c_{\alpha_1}c_{\alpha_2} & s_{\alpha_1}c_{\alpha_2} & s_{\alpha_2} \\ -(c_{\alpha_1}s_{\alpha_2}s_{\alpha_3} + s_{\alpha_1}c_{\alpha_3}) & c_{\alpha_1}c_{\alpha_3} - s_{\alpha_1}s_{\alpha_2}s_{\alpha_3} & c_{\alpha_2}s_{\alpha_3} \\ -c_{\alpha_1}s_{\alpha_2}c_{\alpha_3} + s_{\alpha_1}s_{\alpha_3} & -(c_{\alpha_1}s_{\alpha_3} + s_{\alpha_1}s_{\alpha_2}c_{\alpha_3}) & c_{\alpha_2}c_{\alpha_3} \end{pmatrix}, \tag{2.2}$$

where $\alpha_1, \alpha_2, \alpha_3$ are the three mixing angles, and we use the short-hand notations $s_x = \sin x$, $c_x = \cos x$. The singlet admixture of the physical states are given by $\Sigma_{h_i} = |R_{i3}|^2, i = 1, 2, 3$.

The couplings of the Higgs bosons to SM particles are modified w.r.t. to the couplings of a SM Higgs boson. We express the couplings of the scalar mass eigenstates h_i, normalized

[2] In type II Φ_1 is coupled to leptons and down-type quarks, while Φ_2 is coupled to up-type quarks. In type IV the couplings to quarks are unchanged, but the leptons are coupled to Φ_2 instead of Φ_1.

JHEP08(2022)201

to the corresponding SM couplings, in terms of the coupling coefficients c_{h_iVV} and $c_{h_if\bar{f}}$, such that the couplings to the massive vector bosons are given by

$$(g_{h_iWW})_{\mu\nu} = \mathrm{i} g_{\mu\nu}\,(c_{h_iVV})\,g M_W \quad \text{and} \quad (g_{h_iZZ})_{\mu\nu} = \mathrm{i} g_{\mu\nu}\,(c_{h_iVV})\,\frac{g M_Z}{c_\mathrm{w}}\,, \tag{2.3}$$

where g is the $\mathrm{SU}(2)_L$ gauge coupling, c_w is the cosine of the weak mixing angle, $c_\mathrm{w} = M_W/M_Z$, $s_\mathrm{w} = \sqrt{1-c_\mathrm{w}^2}$, and M_W and M_Z are the masses of the W boson and the Z boson, respectively. The couplings of the Higgs bosons to the fermions are given by

$$g_{h_if\bar{f}} = \frac{m_f}{v}\left(c_{h_if\bar{f}}\right)\,, \tag{2.4}$$

where m_f is the mass of the fermion, and $v = \sqrt{(v_1^2+v_2^2)} \approx 246\,\mathrm{GeV}$ is the SM vev. Analytical expressions for these coupling coefficients in terms of the mixing angles $\alpha_{1,2,3}$ and β can be found in ref. [31].

The scalar potential of the N2HDM comprises 12 parameters. Since the value of v can be determined from the known gauge-boson masses, it can be used to eliminate one degree of freedom, such that 11 free parameters remain. We use the public code `ScannerS` [33, 41, 42], with which the model can be explored in terms of the parameters

$$c^2_{h_2t\bar{t}}\,,\quad c^2_{h_2VV}\,,\quad \mathrm{sign}(R_{23})\,,\quad R_{13}\,,\quad \tan\beta\,,\quad v_S\,,\quad m_{h_{1,2,3}}\,,\quad m_A\,,\quad m_{H^\pm}\,,\quad m^2_{12}\,. \tag{2.5}$$

Here, m_A, $m_{H^\pm}$ denote the masses of the physical CP-odd and charged Higgs bosons, respectively. We will identify the lightest CP-even Higgs boson, h_1, with the one that could potentially be identified with a signal at 95 GeV, labelled h_{95}. The second-lightest CP-even Higgs boson will be identified with the observed state at 125 GeV, labelled h_{125}. Besides the 11 free parameters mentioned above, eq. (2.5) also contains the entry $\mathrm{sign}(R_{23})$, which is used to lift a degeneracy arising from the dependence of the mixing angles α_i on the squared values of the coupling coefficients $c^2_{h_2t\bar{t}}$ and $c^2_{h_2VV}$ and the element of the mixing matrix R_{13}.

3 Theoretical and experimental constraints

In our analysis we apply several theoretical requirements to the parameter space of the N2HDM. In order to ensure that the electroweak minimum of a parameter point is physically viable it is required that it is either stable or meta-stable, where in the latter case the electroweak minimum is not the global minimum of the potential but the electroweak vacuum is sufficiently long-lived in comparison to the age of the universe. In particular, we apply conditions on the scalar couplings that exclude parameter points for which the scalar potential is not bounded from below [33, 43]. Moreover, for parameter points with a meta-stable electroweak minimum we calculate the lifetime of the electroweak vacuum and verify that it is large compared to the lifetime of the universe. For the calculation of the lifetime, `ScannerS` provides an interface to the public code `EVADE` [44, 45] (see also the analysis in ref. [46]). Finally, we apply the tree-level perturbative unitarity conditions that ensure that in the high-energy limit the eigenvalues of the scalar 2×2 scattering matrix are smaller than $|8\pi|$ [33].

JHEP08(2022)201

The parameter space of the N2HDM is also subject to various experimental constraints. We verify the agreement of the selected points with the currently available measurements of the properties of the state that has been discovered at about 125 GeV using the public code `HiggsSignals v.2.6.1` [47–50]. `HiggsSignals` provides a statistical χ^2-analysis of the comparison of the predictions of the considered model with the measurements of the mass, signal strengths and differential information in terms of STXS bins of the state at 125 GeV. In the following we denote as χ^2_{125} the χ^2 contribution obtained from `HiggsSignals`. In our scans, we combine the result for χ^2_{125} with the χ^2-contribution of the fit result arising from confronting the predictions for h_{95} with the observed excesses at about 95 GeV, as we will further specify in section 4.

In order to test the parameter points against the exclusion limits from the Higgs-boson searches at LEP, the Tevatron and in particular from the LHC, we employ the public code `HiggsBounds v.5.9.1` [51–56]. The limits from searches for charged Higgs bosons yield important constraints at low $\tan\beta$ [57]. For larger $\tan\beta$ the searches for heavy Higgs bosons decaying into a pair of τ-leptons play an important role in the type II N2HDM [10, 12, 58]. The recent CMS search [12] (where the $\tau^+\tau^-$ excess in the low-mass region has been observed) is not yet included in `HiggsBounds`. We therefore applied the cross-section limits that were obtained from this search in the high-mass region in a second step in addition to the `HiggsBounds` analysis. The impact on the allowed parameter points turned out to be very small, which is related to the fact that the corresponding ATLAS analysis in the high-mass region which is included in `HiggsBounds` is more sensitive over a large mass range. For intermediate values of $\tan\beta$ the channels with the highest expected sensitivities arise from Higgs cascade decays or bosonic final states including the massive gauge bosons.

Constraints from flavor-physics observables are taken into account by he approach as implemented in `ScannerS`, where the 2HDM flavor constraints projected to the $\tan\beta$–$m_{H^\pm}$ plane as given in ref. [59] are applied under the assumption that the constrains approximately hold in the N2HDM. The flavor constraints lead to a lower limit of $m_{H^\pm} \gtrsim 650$ GeV which is identical in type II and type IV. The lower limit on $\tan\beta$ is somewhat higher in type IV.

Constraints from electroweak precision observables (EWPO) can in a simple approximation be expressed in terms of the oblique parameters S, T and U [60, 61]. Effects from physics beyond the SM on these parameters can be significant if the new physics contributions enter mainly through gauge boson self-energies, as it is the case for extended Higgs sectors. `ScannerS` has implemented the one-loop corrections to the oblique parameters for models with an arbitrary number of Higgs doublets and singlets from ref. [62]. In 2HDMs there is a strong correlation between T and U, and T is the most sensitive of the three oblique parameters. Thus, the contributions to U are much smaller than the ones to T for points that are not excluded by an extremely large value of T [63], and can safely be neglected. Therefore, for points to be in agreement with the experimental observation, we require that the predictions for the S and the T parameters are within the $2\,\sigma$ ellipse of the experimental results, corresponding to $\chi^2 = 6.18$ for two degrees of freedom, making use of the fit result of ref. [59].

JHEP08(2022)201

4 Numerical analysis

In this section we discuss our numerical analysis where we investigate whether the different excesses that were observed near 95 GeV in the searches for additional Higgs bosons can be described in terms of a single new Higgs particle. In the first part presented in section 4.1, we restrict the analysis to the excesses in the $\gamma\gamma$ and the $\tau^+\tau^-$ final states observed by CMS. By comparing the signal rates in the type II and the type IV of the N2HDM, this analysis will demonstrate that only in the type IV N2HDM the state at 95 GeV can give rise to signal rates in the $\gamma\gamma$ and the $\tau^+\tau^-$ final state that are large enough to explain the excesses simultaneously. In the subsequent analysis discussed in section 4.2, in which we consequently focus only on the type IV, we include in addition the LEP excess in the $b\bar{b}$ final state in order to answer the question whether all three excesses can be accommodated simultaneously. We complement the numerical discussion in section 4.3 by investigating the future prospects for experimentally confirming or excluding the proposed scenario. Here we will especially focus on the differences between the parameter regions that describe the two excesses observed by CMS and the ones where all three excesses can simultaneously be described.

4.1 CMS-excesses: $h_{95} \to \gamma\gamma$ and $h_{95} \to \tau^+\tau^-$

As discussed in ref. [31], both the type II and the type IV N2HDM can accommodate the $\gamma\gamma$ excess at 95 GeV. Here we address the question whether in addition the $\tau^+\tau^-$ excess can be explained. To this end, we perform a scan in type II and type IV of the N2HDM over the free parameters as defined in eq. (2.5), where the scan ranges were chosen to be

$$\begin{aligned}
&94\,\text{GeV} \le m_{h_1} \le 98\,\text{GeV}\,, \quad m_{h_2} = 125.09\,\text{GeV}\,, \quad 400\,\text{GeV} \le m_{h_3} \le 1000\,\text{GeV}\,,\\
&\quad 400\,\text{GeV} \le m_A \le 1000\,\text{GeV}\,, \quad 650\,\text{GeV} \le m_{H^\pm} \le 1000\,\text{GeV}\,,\\
&0.5 \le \tan\beta \le 14.5\,, \quad 0\,\text{GeV} \le m_{12}^2 \le 10^6\,\text{GeV}^2\,, \quad 100\,\text{GeV} \le v_S \le 1500\,\text{GeV}\,,\\
&0.6 \le c^2_{h_2VV} \le 1.0\,, \quad 0.6 \le c^2_{h_2t\bar{t}} \le 1.2\,, \quad \text{sign}(R_{13}) = \pm 1\,, \quad -1 \le R_{23} \le 1\,.
\end{aligned} \tag{4.1}$$

For the state $h_1 = h_{95}$ that will be confronted with the observed excesses, we use a mass range that is compatible with the $\gamma\gamma$ excess, since the search in the $\gamma\gamma$ final state has the best mass resolution of the three observed excesses. It should also be noted that we set a lower limit on $m_{H^\pm}$ in view of the constraints from flavor-physics observables (see above). Since mass splittings between the states h_3, A and $H^\pm$ larger than about 200 GeV give rise to large values of the quartic scalar couplings and thus to potential problems with pertubation theory or even Landau poles at energy scales of around 1 TeV [40], we accordingly also limit the scan range of m_A and m_{h_3} via a lower limit of 400 GeV. We use the public code `ScannerS` [33, 41, 42], which scans the parameters randomly over the given range and applies the theoretical and experimental constraints discussed in section 3.[3] `ScannerS` is interfaced to `HiggsBounds` and `HiggsSignals` for the check against the limits from searches for additional Higgs bosons and the constraints from the measured properties

[3] We modified the routines for the check against the EWPO in order to apply a more conservative two-dimensional χ^2-fit to S and T instead of a three-dimensional χ^2-fit to S, T and U.

JHEP08(2022)201

of h_{125}, respectively. The required theoretical predictions for the cross sections and the branching ratios of the scalars are obtained from the public codes `SusHi` [64, 65] and `N2HDECAY` [33, 66–69]. These codes also provide the required input for the computation of the signal rates of the state h_{95}, except for the Higgsstahlung cross section at LEP, which we calculate by a rescaling of the SM prediction with the factor $c^2_{h_{95}VV}$.

In order to analyze whether a simultaneous fit to the observed $\gamma\gamma$ and $\tau^+\tau^-$ excesses is possible, we perform a χ^2-analysis where χ^2 takes into account the two contributions $\chi^2_{\gamma\gamma}$ and $\chi^2_{\tau\tau}$ defined by the measured central values $\mu^{\text{exp}}_{\gamma\gamma,\tau\tau}$ and the $1\,\sigma$ uncertainties $\Delta\mu^{\text{exp}}_{\gamma\gamma,\tau\tau}$ of the signal rates related to the two excesses as specified in eq. (1.1) and eq. (1.3), i.e.

$$\chi^2_{\gamma\gamma,\tau\tau} = \frac{(\mu_{\gamma\gamma,\tau\tau} - \mu^{\text{exp}}_{\gamma\gamma,\tau\tau})^2}{(\Delta\mu^{\text{exp}}_{\gamma\gamma,\tau\tau})^2}\,, \tag{4.2}$$

where $\mu_{\gamma\gamma,\tau\tau}$ are the model predictions. In view of the fact that in the considered extended Higgs sector the properties of h_{95} are closely related to the ones of h_{125}, we also add the contribution χ^2_{125} obtained with the help of `HiggsSignals` in order to ensure that the properties of h_{125} are in agreement with the experimental measurements. We define the total χ^2 as the sum

$$\chi^2 = \chi^2_{\gamma\gamma} + \chi^2_{\tau\tau} + \chi^2_{125}\,. \tag{4.3}$$

In the following we consider a parameter point as acceptable if the condition $\chi^2 \leq \chi^2_{\text{SM}}$ is fulfilled. The χ^2 contribution in the SM, χ^2_{SM}, is obtained for $\mu^{\text{SM}}_{\gamma\gamma} = \mu^{\text{SM}}_{\tau\tau} = 0$, yielding $\chi^2_{\text{SM},\gamma\gamma} = 9.00$ and $\chi^2_{\text{SM},\tau\tau} = 6.17$, while $\chi^2_{\text{SM},125} = 85.77$ results from confronting the properties of a SM Higgs boson at 125 GeV with the experimental measurements using `HiggsSignals`. We will also indicate the best-fit point with the smallest value of χ^2 with a magenta star in our plots. It should be noted in this context that all the remaining experimental constraints are applied on the basis of approximate 95% confidence-level limits, either allowing or excluding a parameter point, instead of including additional contributions in the definition of χ^2 as defined above. This reflects the fact that here we are primarily interested in the collider phenomenology of the two light states Higgs bosons h_{95} and h_{125}.

In figure 1 we show the parameter points of our scan with the predicted values for $\mu_{\gamma\gamma}$ on the horizontal axis and $\mu_{\tau\tau}$ on the vertical axis. The colors of the points indicate the value of χ^2_{125}. In the left plot we show the parameter points for the type II N2HDM, and in the right plot we show the parameter points for the type IV. One can see that only the type IV N2HDM predicts parameter points that fall within the $1\,\sigma$ confidence-region with regards to $\chi^2_{\gamma\gamma+\tau\tau} = \chi^2_{\gamma\gamma} + \chi^2_{\tau\tau}$, where the $1\,\sigma$ region is indicated by the black dashed ellipse in figure 1.[4] On the contrary, parameter points in type II that can accommodate the $\tau^+\tau^-$ excess predict hardly any signal in the $\gamma\gamma$ decay mode, i.e. $\mu_{\gamma\gamma} \lesssim 0.02$ if $\mu_{\tau\tau} \gtrsim 0.3$. As a result, demanding

[4]The fact that effectively all parameter points are located below the observed central value of $\mu^{\text{exp}}_{\tau\tau}$ justifies the choice to use the lower $1\,\sigma$ uncertainty for the cross section in order to define $\mu^{\text{exp}}_{\tau\tau}$ as in eq. (1.3).

JHEP08(2022)201

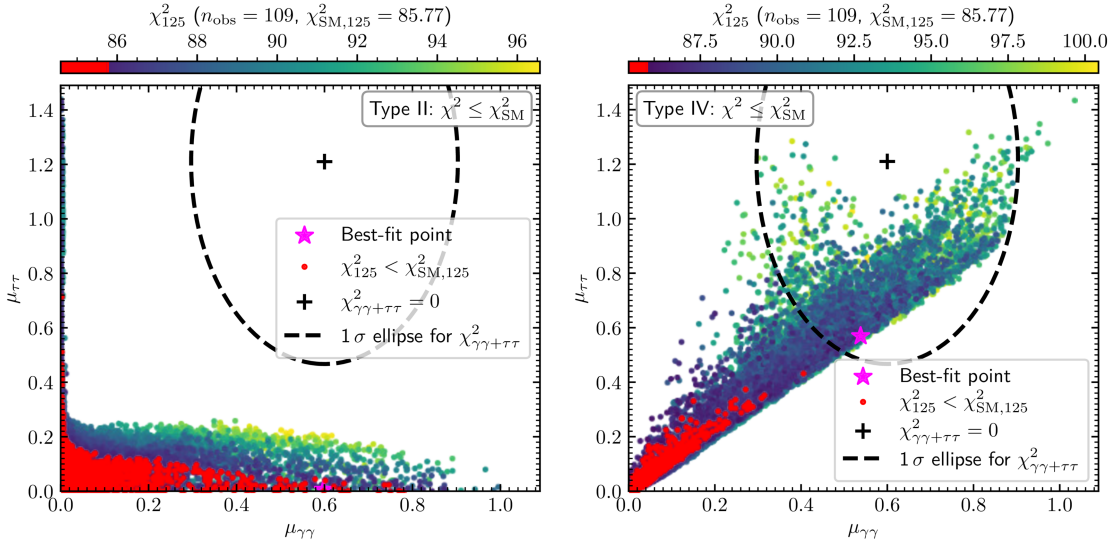

Figure 1. $\mu_{\tau\tau}$ in dependence of $\mu_{\gamma\gamma}$ in the N2HDM type II (left) and type IV (right). The color coding indicates the value of χ^2_{125}. Red points predict $\chi^2_{125} < \chi^2_{\rm SM,125}$. The $1\,\sigma$ confidence-level region with regards to $\chi^2_{\gamma\gamma+\tau\tau}$ is indicated by the dashed black line. The best-fit point is indicated with a magenta star.

that both excesses are fitted simultaneously requires a type IV interpretation, whereas in type II the two excesses cannot be associated with the same particle.[5]

The different results in both Yukawa types of the N2HDM can be understood by realizing that, as explained in more detail in ref. [31], sizable values of $\mu_{\gamma\gamma} \approx \mu^{\rm exp}_{\gamma\gamma}$ require an enhancement of the diphoton branching ratio via a suppression of the $h_{95} \to b\bar{b}$ decay mode. Accordingly, taking into account that $c_{h_{95}b\bar{b}}$ is proportional to c_{α_1} [31], fitting the $\gamma\gamma$ excess is possible in the region where c_{α_1} is small. In type II the down-type quarks and the leptons are coupled to the same Higgs doublet Φ_1. As a consequence, one finds $c_{h_{95}\tau^+\tau^-} = c_{h_{95}b\bar{b}}$, such that also the $h_{95} \to \tau^+\tau^-$ decay mode is suppressed in the parameter region suitable for an explanation of the $\gamma\gamma$ excess. In type IV, on the other hand, the second doublet Φ_2 is coupled to the leptons. Then $c_{h_{95}\tau^+\tau^-}$ is proportional to s_{α_1} (instead of c_{α_1}), and the branching ratio for $h_{95} \to \tau^+\tau^-$ is unsuppressed in the parameter region that allows sizable values of $\mu_{\gamma\gamma}$.

In the plots in figure 1 we have highlighted in red the parameter points that predict $\Delta\chi^2_{125} = \chi^2_{125} - \chi^2_{\rm SM,125} < 0$. Hence, the red points provide an even better description of the measurements of the SM-like Higgs boson h_{125} than the SM. However, we emphasize that the values of $\Delta\chi^2_{125}$ for the red points are so small that they are statistically not significant. It is interesting to note, however, that the red points all lie outside of the $1\,\sigma$ ellipse with regards to $\chi^2_{\gamma\gamma} + \chi^2_{\tau\tau}$. Therefore, small modifications of the properties of h_{125} compared

[5] It remains to be explored whether supersymmetric models with additional singlets (e.g. the NMSSM or the $\mu\nu$SSM) could provide a simultaneous description of the two excesses. In these models potentially large quantum corrections from supersymmetric partners of the SM particles (e.g. in terms of the so-called Δ_b-corrections) could lead to a suppression of the $b\bar{b}$ decay mode, while leaving the $\tau^+\tau^-$ decay mode essentially unsuppressed.

JHEP08(2022)201

to the SM predictions are a feature of the parameter points that fit both excesses. This is also the reason why the best-fit point (magenta star) is located relatively close to the border of the $1\,\sigma$ ellipse, because parameter points located more centrally in the ellipse are associated with slightly larger values of χ^2_{125}. It should be mentioned, however, that there are many points in the $1\,\sigma$ ellipse with $\Delta\chi^2_{125} < 5.99$, which would correspond to a 95% confidence-level exclusion based just on the properties of h_{125} [50].[6] Taking into account the current precision of the signal-rate measurements of h_{125}, the modifications of the theoretical predictions are not large enough to allow for an exclusion of the points inside the ellipse. Nevertheless, future measurements at the HL-LHC or a possible future e^+e^--collider might be able to probe the scenario presented here. We will discuss the future prospects with regards to the coupling measurements of h_{125} in more detail in section 4.3.

Another interesting observation is that even in type IV there are no points which lie at the center of the ellipse, which is indicated by the black cross in figure 1. The reason for this is that such points are excluded by the Higgs-boson searches at LEP in the di-tau final state [6]. It should be noted in this context that also the points to the right of the black cross with $\mu_{\tau\tau} \approx \mu^{\text{exp}}_{\tau\tau}$ and $\mu_{\gamma\gamma} > \mu^{\text{exp}}_{\gamma\gamma}$ would be excluded by the LEP search at the 95% confidence level. However, these parameter points still pass the `HiggsBounds` analysis (and are therefore shown in the plots), because `HiggsBounds` only compares the predictions of the cross sections of each Higgs boson to the most sensitive search based on the *expected* sensitivity of the experimental search in order to ensure the correct statistical interpretation of the obtained bound as a 95% C.L. limit [54]. For the parameter points with values of $\mu_{\gamma\gamma} > \mu^{\text{exp}}_{\gamma\gamma}$ the most sensitive search is the CMS search in the $\gamma\gamma$ final state [9], for which the observed exclusion limit is substantially weaker than the expected limit due to the observed excess. In order to demonstrate the potential impact of the LEP limit in the $\tau^+\tau^-$ final state we show in figure 8 of appendix A the same plot as in figure 1 (right) where we have indicated points that would be excluded by the LEP limit in the $\tau^+\tau^-$ final state if that channel had been selected in order to determine the 95% C.L. limit. It should be noted, however, that requiring the limits from several collider searches to be individually fulfilled at the 95% C.L. leads to a statistical interpretation of the resulting limit that is stronger than an overall 95% C.L.. In order to maintain the statistical interpretation of the applied cross-section limits from BSM Higgs-boson searches as an overall exclusion bound at the 95% C.L., in our analysis we will stick to the approach as implemented in `HiggsBounds`, where only the observed limit is applied that has the highest expected sensitivity.

After having established that the type IV N2HDM can account for a simultaneous explanation of both the $\gamma\gamma$ and the $\tau^+\tau^-$ excesses, but not the Yukawa type II, we now investigate what parameter configurations are most suitable. In figure 2 we show for type IV the parameter points in the same plane as in figure 1, but here the color coding indicates the values of $\tan\beta$ (left plot) and m_{h_3} (right plot). Focusing on the points inside the 1σ ellipse, one can see that parameter points with values of $\tan\beta$ at the upper end of the scan range are located on a diagonal band of points. These points predict the smallest values of

[6] Here it is assumed that the SM prediction $\chi^2_{\text{SM},125}$ is a good estimate of the best-fit value of the type IV N2HDM. This assumption is a good approximation according to the fact that we found $\min(\chi^2_{125}) \approx \chi^2_{\text{SM},125}$ in our scans, as is also visible in the right plot of figure 1 and in figure 3.

JHEP08(2022)201

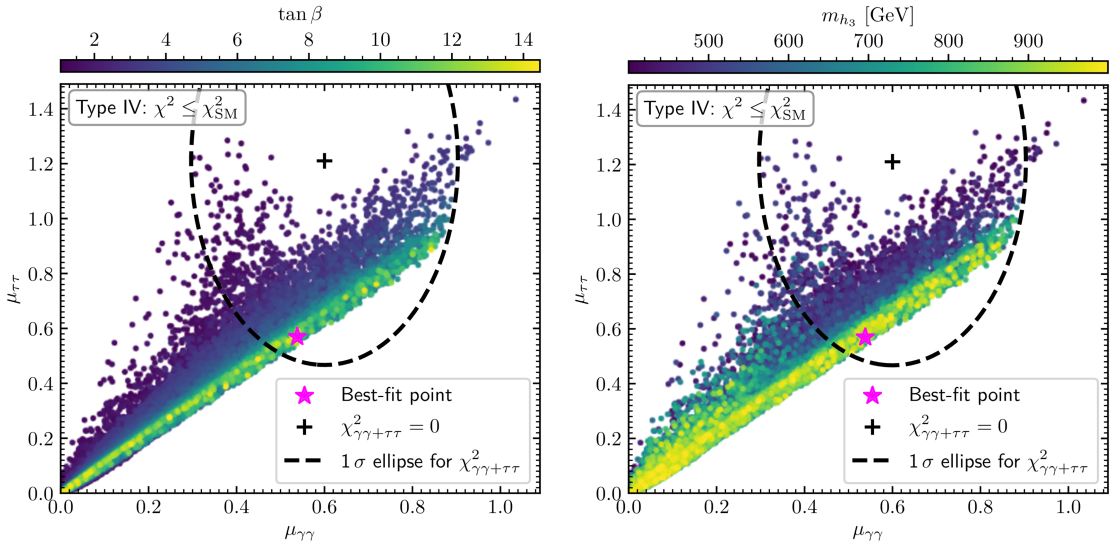

Figure 2. As in figure 1, but the color coding indicates the value of $\tan\beta$ (left) and of m_{h_3} (right).

$\mu_{\tau\tau}$ for a given value of $\mu_{\gamma\gamma}$. Larger values of $\mu_{\tau\tau}$ for fixed $\mu_{\gamma\gamma}$ can be achieved for values of $\tan\beta \lesssim 5$. In the lower range of $\tan\beta$ we find parameter points that reach values of $\mu_{\tau\tau}$ around or above the observed central value $\mu_{\tau\tau}^{\rm exp} = 1.2$. No such preference for smaller values of $\tan\beta$ is observed with regards to $\mu_{\gamma\gamma}$.

In the right plot of figure 2 one can observe that the values of $\mu_{\tau\tau}$ are also correlated with the mass of the heaviest CP-even Higgs boson m_{h_3}. On the diagonal band of points for which we found the points with large values of $\tan\beta$, we find values of m_{h_3} over the whole scan range.[7] The parameter points above this diagonal band that feature the largest values of $\mu_{\tau\tau}$ are only found for values of m_{h_3} at the lower end of the scan range. The fact that sizable values of $\mu_{\tau\tau}$ are associated with relatively small values of $\tan\beta$ and m_{h_3} is caused by an intricate interplay of the various theoretical and experimental constrains which give rise to a correlation between the allowed values of the mixing angles α_i for given values of $\tan\beta$ and m_{h_3}. The correlations between the parameters $\tan\beta$ and m_{h_3} and the signal strength $\mu_{\tau\tau}$ is phenomenologically very interesting in view of the prospects for collider searches of the heavy scalar states. Here it should be noted that in type IV the prospects for discovering h_3, A and $H^\pm$ in the leptonic decay modes $h_3, A \to \tau^+\tau^-$ and $H^\pm \to \tau\nu$ are much worse compared to a type II scenario. While in type II for the heavy states H and A the $b\bar{b}$-associated production and the branching ratio to $\tau\tau$-pairs can be enhanced with increasing values of $\tan\beta$, in type IV the $H, A \to \tau^+\tau^-$ decay mode is suppressed when the $b\bar{b}$-associated production cross section is enhanced. Consequently, in type IV hadronic or bosonic decay modes play a bigger role. We will discuss the experimental prospects from direct searches for the heavy Higgs bosons in more detail in section 4.3.

We complete the discussion of this section by a closer examination of the properties of the best-fit point, which is indicated by a magenta star in the plots. The best-fit point has a

[7] In the right plot of figure 2 points are plotted in ascending order of m_{h_3}.

JHEP08(2022)201

m_{h_1}	m_{h_2}	m_{h_3}	m_A	$m_{H^\pm}$		
95.68	125.09	713.24	811.20	677.38		
$\tan\beta$	α_1	α_2	α_3	m_{12}	v_S	
10.26	1.57	1.22	1.49	221.12	1333.47	
$\mathrm{BR}_{h_1}^{bb}$	$\mathrm{BR}_{h_1}^{gg}$	$\mathrm{BR}_{h_1}^{cc}$	$\mathrm{BR}_{h_1}^{\tau\tau}$	$\mathrm{BR}_{h_1}^{\gamma\gamma}$	$\mathrm{BR}_{h_1}^{WW}$	$\mathrm{BR}_{h_1}^{ZZ}$
0.005	0.348	0.198	0.412	$6.630 \cdot 10^{-3}$	0.025	$3.382 \cdot 10^{-3}$
$\mathrm{BR}_{h_2}^{bb}$	$\mathrm{BR}_{h_2}^{gg}$	$\mathrm{BR}_{h_2}^{cc}$	$\mathrm{BR}_{h_2}^{\tau\tau}$	$\mathrm{BR}_{h_2}^{\gamma\gamma}$	$\mathrm{BR}_{h_2}^{WW}$	$\mathrm{BR}_{h_2}^{ZZ}$
0.553	0.085	0.032	0.069	$2.537 \cdot 10^{-3}$	0.228	0.028
$\mathrm{BR}_{h_3}^{tt}$	$\mathrm{BR}_{h_3}^{bb}$	$\mathrm{BR}_{h_3}^{\tau\tau}$	$\mathrm{BR}_{h_3}^{h_1h_1}$	$\mathrm{BR}_{h_3}^{h_1h_2}$	$\mathrm{BR}_{h_3}^{h_2h_2}$	$\mathrm{BR}_{h_3}^{WW}$
0.123	0.739	0.000	0.002	0.072	0.030	0.022
BR_{A}^{tt}	BR_{A}^{bb}	$\mathrm{BR}_{A}^{\tau\tau}$	$\mathrm{BR}_{A}^{Zh_1}$	$\mathrm{BR}_{A}^{Zh_2}$	$\mathrm{BR}_{A}^{Zh_3}$	$\mathrm{BR}_{A}^{WH^\pm}$
0.053	0.173	0.000	0.024	0.001	0.015	0.734
$\mathrm{BR}_{H^\pm}^{tb}$	$\mathrm{BR}_{H^\pm}^{\tau\nu}$	$\mathrm{BR}_{H^\pm}^{Wh_1}$	$\mathrm{BR}_{H^\pm}^{Wh_2}$			
0.922	0.000	0.073	0.003			

Table 1. Parameters of the best-fit point for which the minimal value of χ^2 is found ($\chi^2 = 88.07$, $\chi^2_{125} = 86.24$) and branching ratios of the scalar particles in the type IV scenario. Dimensionful parameters are given in GeV, and the angles are given in radian.

total χ^2-value of $\chi^2 = 88.07$, which is composed of the contributions related to the excesses, $\chi^2_{\gamma\gamma+\tau\tau} = 1.83$, and the contribution related to the SM-like Higgs boson, $\chi^2_{125} = 86.24$. Thus, the excesses are described at the level of less than $1\,\sigma$, and the properties of h_{125} are practically indistinguishable from the ones of a SM Higgs boson given the current experimental uncertainties. In table 1 we show the scalar masses and the values of the remaining free parameters. One can see that a large branching ratio for the $\gamma\gamma$ decay mode of h_{95} arises because $\alpha_1 \approx \pi/2$, such that for the coupling to b-quarks one finds $c_{h_{95}b\bar{b}} \approx 0$. As a result, also the branching ratio for $h_{95} \to b\bar{b}$ is found to be smaller than 1%. This makes apparent that the best-fit point of the χ^2-analysis of this section would not be suitable for additionally accommodating the LEP excess in the $b\bar{b}$ final state. Regarding the heavy states, we find that the most striking collider signature would be associated to the decay mode $A \to H^\pm W^\mp$. However, given the relatively large values of the masses a discovery at the LHC seems to be not very promising.

4.2 CMS- and LEP-excesses: $h_{95} \to \gamma\gamma$, $h_{95} \to \tau^+\tau^-$ and $h_{95} \to b\bar{b}$

As a next step of our analysis, we take into account also the LEP excess observed at a comparable mass in the $b\bar{b}$ decay mode. Accordingly, we investigate whether the singlet-like scalar h_{95} in the N2HDM of type IV can have signal-rates that are in agreement with the experimentally observed values in three different decay channels and two different production modes, i.e. gluon-fusion production and e^+e^- Higgsstrahlung production. We restrict the analysis to the type IV N2HDM since we demonstrated in the previous section

JHEP08(2022)201

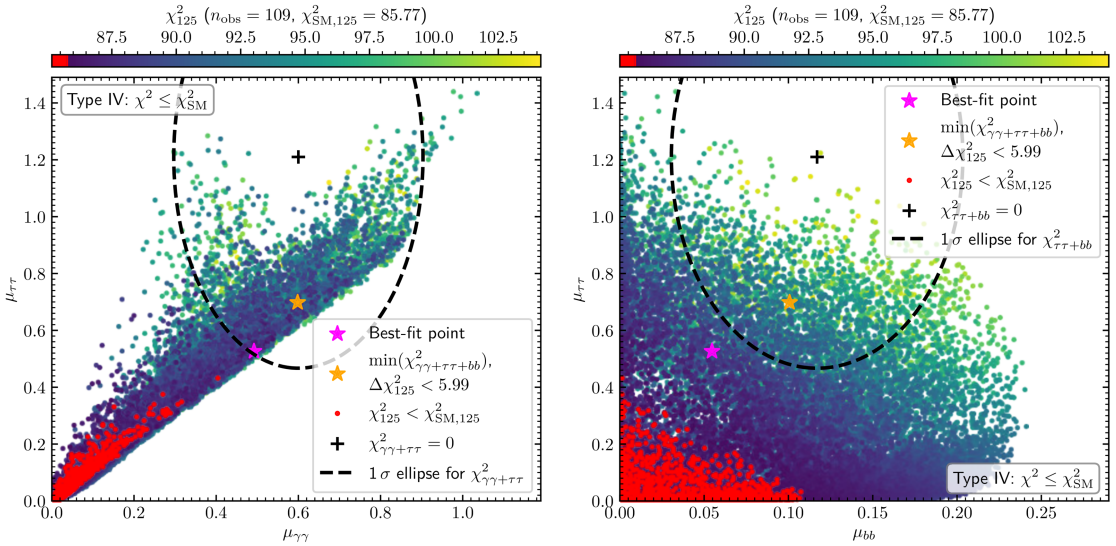

Figure 3. $\mu_{\tau\tau}$ in dependence of $\mu_{\gamma\gamma}$ (left) and μ_{bb} (right). The $1\,\sigma$ confidence-level regions with regard to $\chi^2_{\gamma\gamma} + \chi^2_{\tau\tau}$ (left) and $\chi^2_{bb} + \chi^2_{\tau\tau}$ (right) are indicated by the dashed black line. The color coding is as in figure 1.

that the type II is not capable of accommodating the $\tau^+\tau^-$ excess in combination with the $\gamma\gamma$ excess. We make use of the same set of parameter points that were generated according to the discussion in section 4.1. However, for the present analysis we define the total χ^2 that is investigated via

$$\chi^2 = \chi^2_{\gamma\gamma} + \chi^2_{\tau\tau} + \chi^2_{bb} + \chi^2_{125}\,, \tag{4.4}$$

where the additional contribution

$$\chi^2_{bb} = \frac{(\mu_{bb} - \mu^{\rm exp}_{bb})^2}{(\Delta\mu^{\rm exp}_{bb})^2}\,, \tag{4.5}$$

quantifies the description of the $b\bar{b}$ excess, constructed by means of the theory prediction μ_{bb} and the experimentally measured central value and $1\,\sigma$ uncertainty as shown in eq. (1.2). As before, we consider as valid parameter points the ones that fulfill the condition $\chi^2 < \chi^2_{\rm SM}$, where again $\chi^2_{\rm SM}$ is evaluated assuming no signal contribution to the excesses at 95 GeV, such that $\chi^2_{{\rm SM},bb} = 4.21$. The condition $\chi^2 < \chi^2_{\rm SM}$ allows for rather larger values of $\Delta\chi^2_{125} \gtrsim 15$ for parameter points that fit all three excesses at 1σ or below, i.e. $\chi^2_{\gamma\gamma+\tau\tau+bb} = \chi^2_{\gamma\gamma} + \chi^2_{\tau\tau} + \chi^2_{bb} < 3.53$. In order to ensure that there are parameter points that fit the excesses and which are not significantly disfavoured by the experimental data related to h_{125}, we will therefore also show results under the additional constraint $\Delta\chi^2_{125} < 5.99$.

In the left plot of figure 3 we show the parameter points in the $\mu_{\gamma\gamma}$–$\mu_{\tau\tau}$ plane, with the color coding indicating the value of χ^2_{125}. This plot can be compared to the right plot of figure 1 from the analysis discussed in section 4.1. One can see that the distribution of the points is very similar in both plots. This indicates that the inclusion of χ^2_{bb} has no significant impact on the values of $\mu_{\gamma\gamma}$ and $\mu_{\tau\tau}$ that can be achieved while respecting the condition $\chi^2 < \chi^2_{\rm SM}$. However, the best-fit point, indicated with the magenta star, has changed, and it

JHEP08(2022)201

is located further away from the center of the $1\,\sigma$ ellipse. This indicates that the parameter points that have a better agreement with the observed signal rates of the excesses are associated with a χ^2-penalty from the properties of h_{125} contained in χ^2_{125}. In order to shed light on whether it is possible to describe the excesses sufficiently well without being in significant tension with the signal-rate measurements of h_{125}, we indicate with the orange star the parameter point with the minimum value of $\chi^2_{\gamma\gamma+\tau\tau+bb} = \chi^2_{\gamma\gamma} + \chi^2_{\tau\tau} + \chi^2_{bb}$ while additionally fulfilling the condition $\Delta\chi^2_{125} < 5.99$. One can see that the orange star is located within the $1\,\sigma$ ellipse regarding the two-dimensional χ^2-distribution $\chi^2_{\gamma\gamma+\tau\tau} = \chi^2_{\gamma\gamma} + \chi^2_{\tau\tau}$, indicating a good description of both excesses. As for the case of the right plot of figure 1, we show in the left plot of figure 9 in appendix A the same plot as in figure 3 (left) where we have indicated in grey points that would be excluded by the LEP limit in the $\tau^+\tau^-$ final state if that channel had been selected in order to determine the 95% C.L. limit.

In the right plot of figure 3 we show the parameter points in the μ_{bb}–$\mu_{\tau\tau}$ plane, with the same color coding as in the left plot. The black ellipse in the right plot shows the $1\,\sigma$ region with regards to $\chi^2_{bb+\tau\tau} = \chi^2_{bb} + \chi^2_{\tau\tau}$. One can see that many points lie within the 1σ ellipse. Thus, both the $b\bar{b}$ excess and the $\tau^+\tau^-$ excess can be accommodated simultaneously. Moreover, the orange star, defined as described above, lies within the ellipse. Since the orange star also lies within the ellipse in the left plot of figure 3 one can conclude that there are points which give rise to a good description of all three excesses, without being in tension with the experimental data related to the SM-like Higgs boson h_{125}. However, the best-fit point lies outside of the 1σ ellipse in the right plot of figure 3. Accordingly, it can also be observed that the values of χ^2_{125} grow with increasing values of the signal-strength μ_{bb} and $\mu_{\tau^+\tau^-}$. This tendency is mainly related to the couplings of h_{95} and h_{125} to vector bosons, which fulfill the sum rule $c^2_{h_{95}VV} + c^2_{h_{125}VV} \approx 1$ taking into account that the vector-boson coupling of the heavy state h_3 is negligible. In order to account for the LEP excess, the Higgsstrahlung production is sufficiently large if $c^2_{h_{95}VV} \approx 0.117/\mathrm{BR}^{bb}_{h_{95}}$ (see eq. (1.2)). This means that depending on the branching ratio for $h_{95} \to b\bar{b}$ the value of $c^2_{h_{125}VV}$ is suppressed by at least 10%. Since the $h_{95} \to \tau^+\tau^-$ decay mode competes with the decay into $b\bar{b}$, a sizable value of $\mu_{\tau\tau}$ requires an even larger value of $c^2_{h_{95}VV}$ in order to fit the $b\bar{b}$ excess, which further suppresses the value of $c^2_{h_{125}VV}$ and strengthens the tension with the measured signal rates of h_{125}. Hence, we expect to observe larger modifications of the properties of h_{125} compared to the SM predictions in this scenario compared to the previous scenario discussed in section 4.1 in which the $b\bar{b}$ excess was not considered. As for the case of the left plot of this figure, we show in the right plot of figure 9 in appendix A the same plot as in figure 3 (right) where we have indicated in grey points that would be excluded by the LEP limit in the $\tau^+\tau^-$ final state if that channel had been selected in order to determine the 95% C.L. limit.

To further scrutinize the relations between the signal rates of the state h_{95} among themselves and also between the former and the properties of the state h_{125}, we show in figure 4 the correlations of $\mu_{\gamma\gamma}$, $\mu_{\tau\tau}$, μ_{bb} and $c^2_{h_{125}VV}$. In these plots the parameter points are shown in three different colors. The grey points are points that do not fit the excesses inside of the three-dimensional $1\,\sigma$ ellipsoid corresponding to $\chi^2_{\gamma\gamma+\tau\tau+bb} \leq 3.53$ and are therefore not further discussed in the following. The blue points are points inside

JHEP08(2022)201

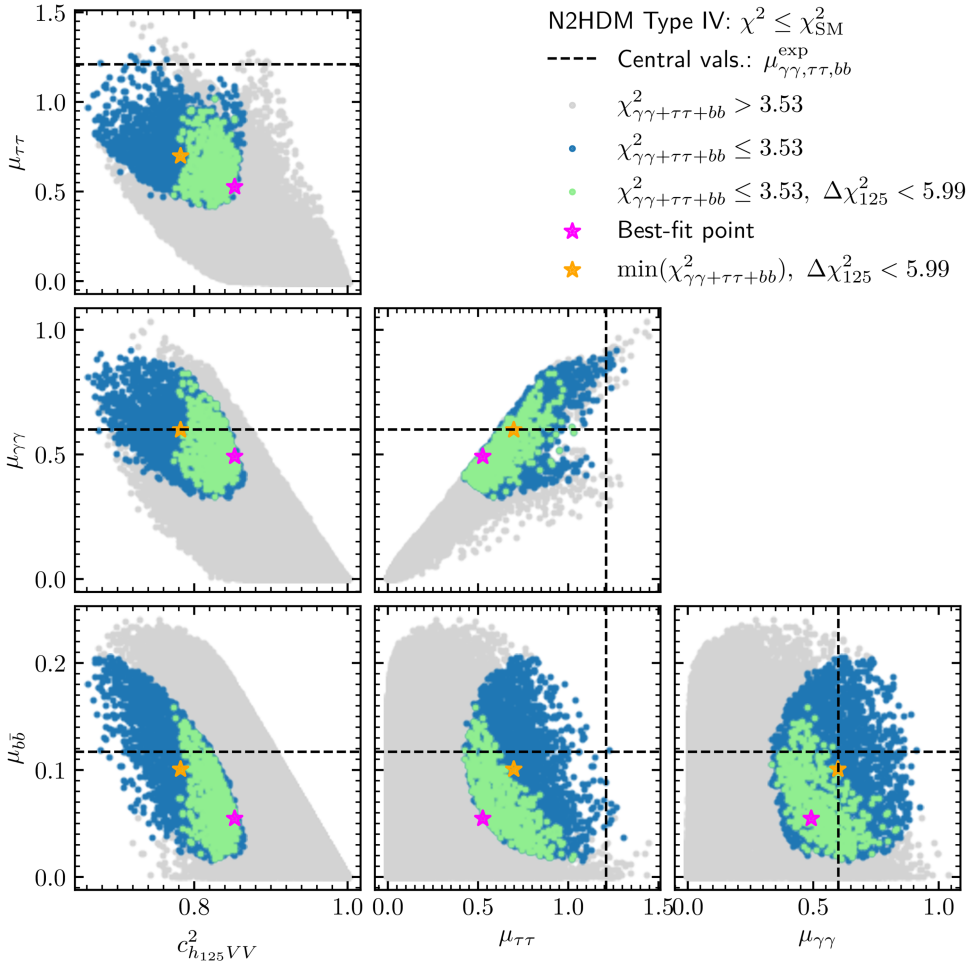

Figure 4. Correlations between the signal rates $\mu_{\tau\tau}$, $\mu_{\gamma\gamma}$ and $\mu_{b\bar{b}}$, and the coupling coefficient $c^2_{h_{125}VV}$. Parameter points that fit the excesses within a three-dimensional confidence level of $1\,\sigma$ are shown in blue, whereas the remaining points are shown in grey. Green points fit the excesses within a confidence level of $1\,\sigma$ and additionally fulfill the condition $\Delta\chi^2_{125} < 5.99$. The best-fit point ($\chi^2 = 90.86$, $\chi^2_{125} = 87.40$) is indicated with a magenta star. The orange star ($\chi^2 = 92.66$, $\chi^2_{125} = 91.46$) indicates the point with the minimal value of $\chi^2_{\gamma\gamma+\tau\tau+bb}$ under the condition that $\Delta\chi^2_{125} < 5.99$.

the $1\,\sigma$ preferred regions according to the observed values of $\mu_{\gamma\gamma}$, $\mu_{\tau\tau}$ and μ_{bb}, i.e. they feature $\chi^2_{\gamma\gamma+\tau\tau+bb} < 3.53$. Finally, the green points are the subset of the blue points that additionally fulfill the condition $\Delta\chi^2_{125} < 5.99$, and as such they do not feature large modifications of the signal rates of h_{125} in view of the current experimental uncertainties. One can see that for all three excesses there are blue points that reach the experimentally observed central values of the signal strengths. However, the experimental central value of $\mu_{\tau\tau}$ cannot be reached when the additional constraint on $\Delta\chi^2_{125}$ is considered, as can bee seen in the plot in the first row. In the lower right plot one can furthermore see that the central values of both $\mu_{\gamma\gamma}$ and μ_{bb} can be reached simultaneously. In the lower center plot, on the other hand, there are blue points that reproduce the central values of $\mu_{\tau\tau}$ and

JHEP08(2022)201

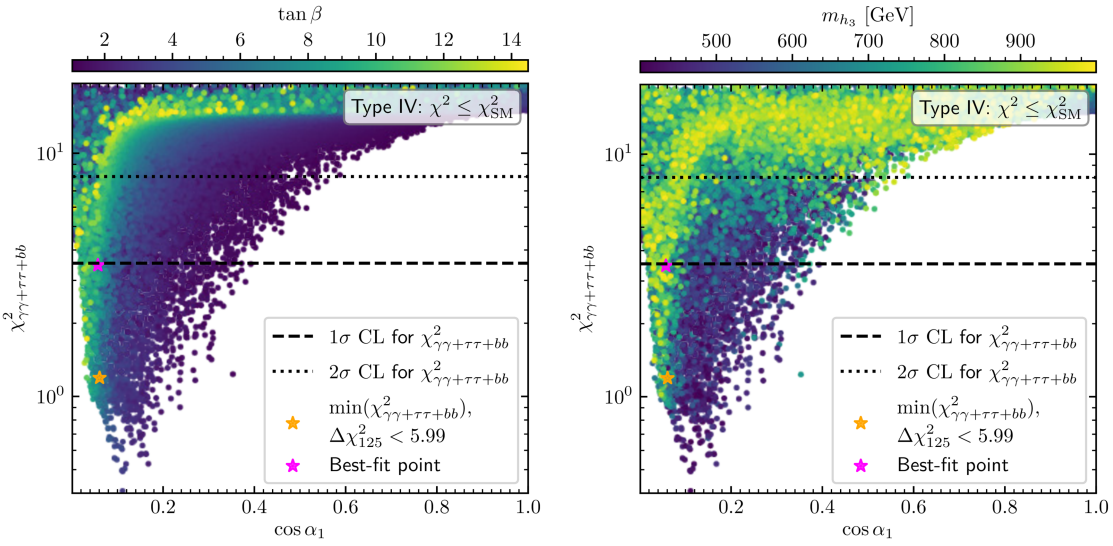

Figure 5. $\chi^2_{\gamma\gamma+\tau\tau+bb}$ in dependence of $\cos\alpha_1$. The color coding indicates the values of $\tan\beta$ (left) and m_{h_3} (right). The magenta and orange stars are defined as in figure 3. The horizontal dashed and dotted lines indicate the $1\,\sigma$ and the $2\,\sigma$ regions, respectively.

μ_{bb}, but the green points feature smaller values of either $\mu_{\tau\tau}$ or μ_{bb}. Finally, in the right plot in the second row there are both blue and green points in the vicinity of the central values of $\mu_{\tau\tau}$ and $\mu_{\gamma\gamma}$. However, no points are found exactly at the central values due to the exclusion limits of the LEP search $ee \to Z(h \to \tau^+\tau^-)$, as already discussed in section 4.1.

Regarding the values of $c^2_{h_{125}VV}$ that are preferred by the excesses, one can see that only for $c^2_{h_{125}VV} \lesssim 0.86$ there are points that fit the excesses sufficiently well. While there are blue points in the range $0.66 \lesssim c^2_{h_{125}VV} \lesssim 0.86$, the green points stretch over a substantially reduced interval of $0.76 \lesssim c^2_{h_{125}VV} \lesssim 0.86$. It is also interesting to compare the maximum value of $c^2_{h_{125}VV}$ for which each excess on its own can be accommodated, and how these numbers compare to the case where all three excesses are fitted together. One can see by comparing the plots in the first column that values of $c^2_{h_{125}VV} \approx 0.90$ are sufficiently small in order to fit the central value of the signal strength of the $b\bar{b}$ excess individually, and a somewhat smaller value of $c^2_{h_{125}VV} \approx 0.88$ is required for the central value of the $\gamma\gamma$ excess. These values are slightly above the range of $c^2_{h_{125}VV}$ for which the excesses can be fitted simultaneously. The relatively large modifications of the couplings of h_{125} compared to the SM prediction are a clear collider target that can be explored at the high-luminosity phase of the LHC or at possible future lepton colliders, as will be discussed in more detail in section 4.3.

We finish this section with a discussion of the values of $\chi^2_{\gamma\gamma+\tau\tau+bb}$ that we found in our scan and of the parameter region where the best description of the excesses has been achieved. In figure 5 we show the distribution of $\chi^2_{\gamma\gamma+\tau\tau+bb}$ in dependence of $\cos\alpha_1$. As discussed in ref. [31] (and also in section 4.1 above), both the $\gamma\gamma$ excess and the $\tau^+\tau^-$ excess require small values of $\cos\alpha_1$ in order to enhance the branching ratios of the decay modes $h_{95} \to \gamma\gamma, \tau^+\tau^-$. For that reason, we find values of $\chi^2_{\gamma\gamma+\tau\tau+bb} < 3.53$, corresponding

JHEP08(2022)201

m_{h_1}	m_{h_2}	m_{h_3}	m_A	$m_{H^\pm}$		
96.47	125.09	733.28	705.87	776.61		
$\tan\beta$	α_1	α_2	α_3	m_{12}	v_S	
6.54	−1.51	−1.08	−1.41	283.92	1244.58	
$\mathrm{BR}^{bb}_{h_1}$	$\mathrm{BR}^{gg}_{h_1}$	$\mathrm{BR}^{cc}_{h_1}$	$\mathrm{BR}^{\tau\tau}_{h_1}$	$\mathrm{BR}^{\gamma\gamma}_{h_1}$	$\mathrm{BR}^{WW}_{h_1}$	$\mathrm{BR}^{ZZ}_{h_1}$
0.377	0.230	0.120	0.250	$3.714 \cdot 10^{-3}$	0.016	$2.116 \cdot 10^{-3}$
$\mathrm{BR}^{bb}_{h_2}$	$\mathrm{BR}^{gg}_{h_2}$	$\mathrm{BR}^{cc}_{h_2}$	$\mathrm{BR}^{\tau\tau}_{h_2}$	$\mathrm{BR}^{\gamma\gamma}_{h_2}$	$\mathrm{BR}^{WW}_{h_2}$	$\mathrm{BR}^{ZZ}_{h_2}$
0.489	0.099	0.036	0.079	$2.808 \cdot 10^{-3}$	0.259	0.032
$\mathrm{BR}^{tt}_{h_3}$	$\mathrm{BR}^{bb}_{h_3}$	$\mathrm{BR}^{\tau\tau}_{h_3}$	$\mathrm{BR}^{h_1h_1}_{h_3}$	$\mathrm{BR}^{h_1h_2}_{h_3}$	$\mathrm{BR}^{h_2h_2}_{h_3}$	$\mathrm{BR}^{WW}_{h_3}$
0.067	0.150	0.000	0.002	0.318	0.182	0.188
BR^{tt}_{A}	BR^{bb}_{A}	$\mathrm{BR}^{\tau\tau}_{A}$	$\mathrm{BR}^{Zh_1}_{A}$	$\mathrm{BR}^{Zh_2}_{A}$		
0.337	0.185	0.000	0.450	0.027		
$\mathrm{BR}^{tb}_{H^\pm}$	$\mathrm{BR}^{\tau\nu}_{H^\pm}$	$\mathrm{BR}^{Wh_1}_{H^\pm}$	$\mathrm{BR}^{Wh_2}_{H^\pm}$			
0.450	0.000	0.516	0.031			

Table 2. Parameters for the point for which the minimal value of $\chi^2_{\gamma\gamma+\tau\tau+bb}$ is found under the condition that $\Delta\chi^2_{125} < 5.99$ (orange star, $\chi^2 = 92.66$, $\chi^2_{125} = 91.47$). Also shown are the branching ratios of the scalar particles. Dimensionful parameters are given in GeV, and the angles are given in radian.

to the $1\,\sigma$ region, at the lower range of $\cos\alpha_1$. However, for the smallest values of $\cos\alpha_1$ the values of $\chi^2_{\gamma\gamma+\tau\tau+bb}$ increase drastically. The reason is that here the decay mode $h_{95} \to b\bar{b}$ has a tiny branching ratio, and the $b\bar{b}$ excess is therefore not accounted for. In the range $\cos\alpha_1 \gtrsim 0.1$ we only find parameter points with values of $\tan\beta$ at the lower end of the scan range. These are also the points which have the smallest value of $\chi^2_{\gamma\gamma+\tau\tau+bb}$, with a minimum at $\chi^2_{\gamma\gamma+\tau\tau+bb} \approx 0.5$. The orange star, indicating the parameter point with minimal value of $\chi^2_{\gamma\gamma+\tau\tau+bb}$ while fulfilling $\Delta\chi^2_{125} < 5.99$, is located well below the $1\,\sigma$ level $\chi^2_{\gamma\gamma+\tau\tau+bb} = 3.53$. In the right plot of figure 5 the color coding indicates the value of m_{h_3}. One can see a similar correlation between $\cos\alpha_1$ and m_{h_3} as in the left plot for $\tan\beta$: only parameter points for which m_{h_3} has a value at the lower end of the scan range lie below the $1\,\sigma$ level for $\cos\alpha_1 \gtrsim 0.1$. On the other hand, for smaller values of $\cos\alpha_1$, there are points covering the whole scan range of m_{h_3} in the $1\,\sigma$ region, where larger values of m_{h_3} correlate with larger values of $\tan\beta$.

In order to provide a concrete example of a parameter point that fits the three excesses, we show in table 2 the spectrum and the other free parameters of the parameter point indicated with the orange star in the plots. This parameter point predicts

$$\bigstar \quad \mu_{\gamma\gamma} = 0.60 \quad \mu_{\tau\tau} = 0.70 \quad \mu_{bb} = 0.10\,. \tag{4.6}$$

This results in a total χ^2-value of $\chi^2 = 92.66$, where $\chi^2_{125} = 91.47$. It is interesting to compare the branching ratios of h_{95} to the ones that we found for the best-fit point in

JHEP08(2022)201

the analysis discussed in section 4.1 in which the $b\bar{b}$ excess was not taken into account. In that case we found a best-fit point for which the branching ratio for the decay mode $h_{95} \to b\bar{b}$ is vanishing due to $\alpha_1 \approx \pi/2$, whereas in the parameter point shown in table 2 the branching ratio for the decay into $b\bar{b}$ is still sizable since $|\alpha_1|$ is slightly smaller. Another important difference concerns the branching ratios of the heavier states. While for the best-fit point from section 4.1 the branching ratios for the decays of h_3, A and $H^\pm$ into final states including h_{95} are small, here we find that A and $H^\pm$ decay with roughly 50% probability into h_{95} plus a gauge boson, and h_3 decays with a probability of about 50% into $h_{95}h_{125}$- or $h_{125}h_{125}$-pairs. These decay signatures are potentially accessible and already searched for at the LHC [70–76]. These searches therefore offer good prospects for future tests of the considered scenario with a particle state at 95 GeV that gives a good description of the excesses.

4.3 Future prospects

In our previous discussion we already touched upon ways to indirectly or directly test the existence of the hypothesized state at 95 GeV. In this section we give concrete examples as to where deviations from the SM predictions might show up in future collider experiments. We start by discussing the modifications of the couplings of the SM-like Higgs boson at 125 GeV. Afterwards, we discuss how the scenarios discussed above can be probed via direct searches for BSM Higgs bosons.

In figure 6 we show the effective coupling coefficients $c_{h_{125}\tau\tau}$ and $c_{h_{125}VV}$ for the parameter points discussed in section 4.1 (i.e., the points fitting the $\gamma\gamma$ and the $\tau^+\tau^-$ excesses) in the left plot and for the scan points of the discussion in section 4.2 (i.e., also fitting the $b\bar{b}$ excess) in the right plot. The parameter points are shown in three different colors. The grey points do not provide a fit to the excesses that were considered in each scan within the 1σ region of the respective χ^2-function. On the other hand, the parameter points depicted in blue describe the excesses at a level of 1σ or below, i.e. the blue points in the left plot feature $\chi^2_{\gamma\gamma+\tau\tau} \leq 2.30$, and the blue points in the right plot feature $\chi^2_{\gamma\gamma+\tau\tau+bb} \leq 3.53$. The points shown in green (as a subset of the blue points) furthermore fulfill the condition $\Delta\chi^2_{125} \leq 5.99$. The plots also show the current 1σ uncertainties of the measurements of the coupling coefficients from ATLAS [77] and CMS [78] indicated by the dotted and the dash-dotted lines, respectively. Furthermore, the plots contain the magenta and the green ellipse which indicate the prospects for these uncertainties after the high-luminosity phase of the LHC [79] and after a hypothetical ILC run at a center-of-mass energy of 250 GeV [80], respectively. The ellipses are placed such that their center lies at the SM prediction in order to visualize the deviations of the couplings predicted by the scan points compared to the SM prediction. However, we emphasize that the placement of the ellipses is based on a hypothetical scenario in which the future experiments will measure no deviations from the SM.

One can see that in both plots the blue points lie a significant amount away from the magenta ellipse. As a consequence, independently of whether the LEP excess is considered or not, the scenarios that describe the CMS excesses predict modifications of the couplings of h_{125} compared to the SM prediction that would be observable at the HL-LHC. The discrepancy to the SM predictions would be even more striking at the ILC. Regarding a

JHEP08(2022)201

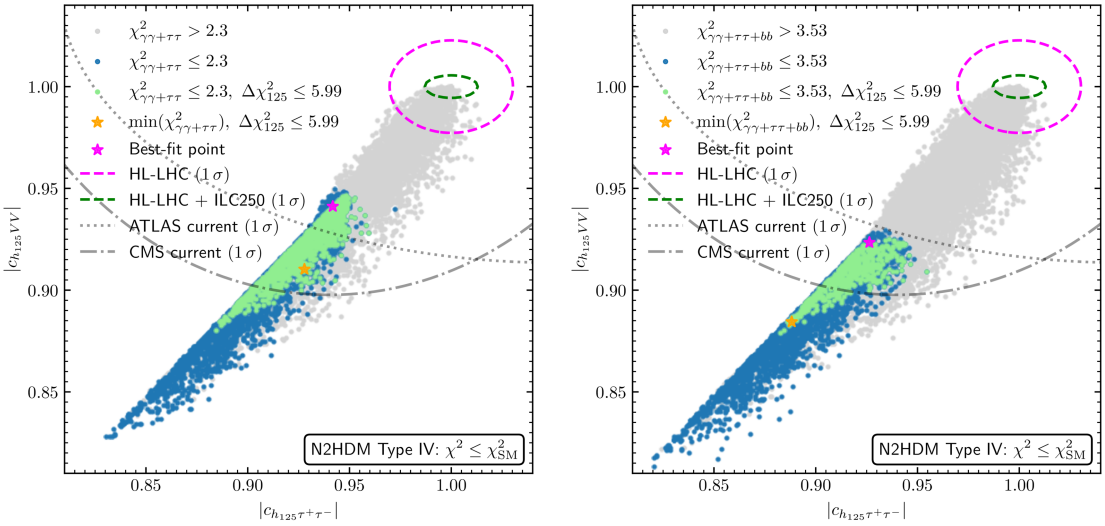

Figure 6. The $|c_{h_{125}VV}|$–$|c_{h_{125}\tau\tau}|$ plane for the parameter points discussed in section 4.1 in the left plot and for the parameter points discussed in section 4.2 in the right plot, respectively. The grey points feature values of $\chi^2_{\gamma\gamma+\tau\tau} > 2.3$ (left) and $\chi^2_{\gamma\gamma+\tau\tau+bb} > 3.53$ (right), whereas the blue points feature $\chi^2_{\gamma\gamma+\tau\tau} \leq 2.3$ (left) and $\chi^2_{\gamma\gamma+\tau\tau+bb} \leq 3.53$ (right). The green points are a subset of the blue points that furthermore feature $\Delta\chi^2_{125} \leq 5.99$. The magenta and orange stars are defined as in figure 3. Also shown are the current $1\,\sigma$ uncertainties of the measurements of the coupling coefficients from ATLAS [77] and CMS [78] indicated by the dotted and the dash-dotted lines, respectively. The magenta and the green ellipse indicate the prospects for these uncertainties after the high-luminosity phase of the LHC [79] and after a hypothetical ILC run at a center-of-mass energy of 250 GeV, respectively [80].

future lepton-collider it should also be taken into account that there the state at 95 GeV could be probed directly, such that the indirect constraints from the properties of h_{125} would complement the results from the direct search for the state at 95 GeV. In fact, the interplay between the results for the couplings of h_{95} and h_{125} will be essential in order to determine which underlying model could be realized in nature. In order to achieve this goal, the higher precision of the coupling measurements of h_{125} at a future e^+e^- collider will be crucial.

We now turn to the direct searches for BSM Higgs bosons in the scenarios that we consider in this paper. The fact that one can continue to search for the state at 95 GeV in the channels in which the excesses were observed is self-evident. However, there is also the interesting possibility to shed light on the presence of h_{95} in a complementary way via searches for the heavier states h_3, A and $H^\pm$. We found that it is most promising to search for the third CP-even state h_3 due to the preferred relatively low values of its mass (see the discussion in section 4.1). The searches for neutral Higgs bosons decaying into a pair of top quarks are sensitive to the presence of h_3 for values of $\tan\beta \approx 1$ and masses of h_3 not too far above the $t\bar{t}$ threshold [81].[8] Searches for the state h_3 with a mass in the range

[8] A local excess of $3.5\,\sigma$ has been observed in ref. [81] for masses of about 400 GeV, which coincides with the preferred mass range of h_3 found in this analysis. However, the shape of the excess favours an interpretation in the form of a CP-odd Higgs boson decaying into a top-quark pair (see ref. [39] for an N2HDM interpretation).

JHEP08(2022)201

$400\,\text{GeV} \lesssim m_{h_3} \lesssim 700\,\text{GeV}$ can also be carried out in the gluon-fusion production mode with subsequent decay into a pair of vector bosons in the low-$\tan\beta$ range [82, 83]. In addition to these conventional collider signatures, there is also the possibility for collider signatures that involve two BSM states. The combined constraints from flavour-physics observables and the EWPO give rise to a mass hierarchy of the form $m_{h_3} < m_A \approx m_{H^\pm} \approx 650\,\text{GeV}$. This hierarchy allows for Higgs cascade decays of the form $A \to Zh_3$ and $H^\pm \to W^\pm h_3$, whose branching ratios can be sizable even in the alignment limit of the N2HDM. The CP-odd state A can be produced for small values of $\tan\beta$ in the gluon-fusion production mode and for large values of $\tan\beta$ in the $b\bar{b}$-associated production mode. As a result, future LHC searches utilizing the signature $A \to h_3 Z$ could probe the N2HDM type IV scenario over the whole scan range of $\tan\beta$. Incidentally, the mass hierarchy $m_{h_3} < m_A \approx m_{H^\pm}$ in combination with low values of $\tan\beta$ can also facilitate the realization of a first-order electroweak phase transition and electroweak baryogenesis in the N2HDM [84].[9] Finally, for the lower scan range of m_{h_3} also the decay mode $h_3 \to h_{125}h_{125}$ becomes important. This signature has been searched for in the final state with four b-quarks [85, 86] and in a final state with a pair of b-quarks and a diphoton pair [87], and can be further probed at the (HL-)LHC.

5 Conclusions

We analyzed local excesses of about $3\,\sigma$ each in the di-photon and the di-tau decay modes near 95 GeV as reported by CMS, by themselves and together with a long-standing $2\,\sigma$ local excess in the $b\bar{b}$ final state that was observed at LEP in a mass range that turns out to be compatible with the excesses observed by CMS.[10] We have investigated whether the observed excesses could be interpreted as arising from a Higgs boson in the 2 Higgs Doublet Model with an additional real Higgs singlet (N2HDM). While in a previous analysis [31] it had been found that the N2HDM of type II and type IV can describe the $\gamma\gamma$- and the $b\bar{b}$-excess simultaneously, we have found that the incorporation of the recently observed excess in the $\tau^+\tau^-$ decay mode can be well accommodated in the N2HDM but yields a clear preference for the type IV Yukawa structure.

Regarding a simultaneous description of the $\gamma\gamma$-excess and the $\tau^+\tau^-$-excess by means of a singlet-like Higgs boson with a mass of about 95 GeV, we have found that the type IV Yukawa structure allows a very good description while being in agreement with the measurements of the properties of the observed Higgs state at 125 GeV and further experimental and theoretical constraints. On the other hand, in the N2HDM type II a simultaneous description of the excesses in the $\gamma\gamma$ and $\tau^+\tau^-$ channels is not possible. Focusing on the type IV N2HDM, we have demonstrated in a second step that one can accommodate also the $b\bar{b}$-excess observed at LEP together with the two excesses observed at CMS. As a summary of this result, we show in figure 7 the signal rates of the state at 95 GeV for

[9] A first-order phase transition can also give rise to a gravitational-wave background that might be detectable in the future.

[10] The fact that all three excesses are found roughly at the same mass value should reduce the impact of the "look-elsewhere" effect (the difference between local and global significance).

JHEP08(2022)201

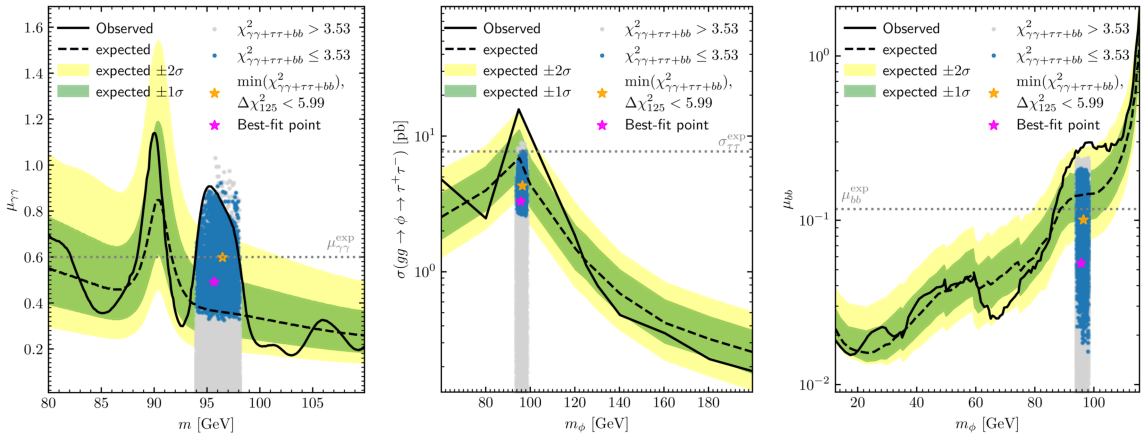

Figure 7. Predicted signal rates $\mu_{\gamma\gamma}$ and μ_{bb} (left and right plots) and cross sections $\sigma_{\tau\tau}$ (middle plot) with regards to the three observed excesses. Blue points feature $\chi^2_{\gamma\gamma+\tau\tau+bb} \leq 3.53$ and describe the excesses at the level of $1\,\sigma$ or better, whereas the grey points feature $\chi^2_{\gamma\gamma+\tau\tau+bb} > 3.53$. The magenta and orange stars are defined as in figure 3. Also shown are the experimentally observed and expected upper limits at the 95% confidence level. The green and yellow bands indicate the 68% and 95% intervals for the expected exclusion limit. The horizontal grey dotted lines indicate the central values of the observed signal strengths/cross section of the three excesses.

the three collider processes in which the excesses were found including the corresponding expected and observed 95% confidence-level exclusion limits of each search [5, 9, 12]. Here the parameter points that describe the three excesses at a level of $1\,\sigma$ or better are shown in blue, whereas the remaining parameter points are shown in grey. One can see that a large set of parameter points yields a good description of the observed excesses, while being in agreement with the theoretical and experimental constraints on the model parameters. In particular, we have verified that a description of the excesses is possible without large modifications of the measured signal rates of the Higgs boson at 125 GeV that would be in disagreement with the current experimental results.

There are various ways by which future collider experiments can shed more light on whether the observed experimental "anomalies" at 95 GeV have indeed a BSM particle origin. Direct searches for the state at 95 GeV at the LHC in the $\gamma\gamma$ and the $\tau^+\tau^-$ final states will obviously be crucial. We are eagerly awaiting the updated results in the $\gamma\gamma$ decay mode by CMS utilizing the full Run 2 dataset. If further evidence will be present in this search after the inclusion of the remaining Run 2 data, the combined statistical significance of the various excesses could indicate a striking indication for new physics. With regard to the $\tau^+\tau^-$ decay mode, we note once more that ATLAS results in the low-mass Higgs-boson searches utilizing the $\tau^+\tau^-$ decay mode are yet to be published. In addition to the direct searches, we emphasized that improved measurements of the properties of the observed Higgs boson at 125 GeV have the potential to probe the N2HDM scenarios presented here. The future precision of the couplings measurements of h_{125} at the high-luminosity phase of the LHC will be sufficient to exclude or confirm the N2HDM scenarios discussed here with respect to the SM at the 95% confidence-level or more. At an e^+e^- Higgs factory running

JHEP08(2022)201

at $\sqrt{s} = 250\,\text{GeV}$ the state h_{95} could be produced copiously, and the measurements of the couplings of both the state at 95 GeV and 125 GeV could shed further light on the underlying model and its parameter space. Finally, we discussed that there are good prospects for a discovery of one or more of the heavier Higgs bosons at the HL-LHC.

Acknowledgments

The work of S.H. is supported in part by the grant PID2019-110058GB-C21 funded by "ERDF A way of making Europe" and by MCIN/AEI/10.13039/501100011033, and in part by the grant CEX2020-001007-S funded by MCIN/AEI/10.13039/501100011033. The work of T.B. and G.W. is supported by the Deutsche Forschungsgemeinschaft under Germany's Excellence Strategy EXC2121 "Quantum Universe" — 390833306. This work has been partially funded by the Deutsche Forschungsgemeinschaft (DFG, German Research Foundation) — 491245950.

A Additional application of the limits from the LEP $\tau^+\tau^-$ searches

As discussed in the context of our results shown in figure 1 and figure 3, parts of the parameter space investigated in our numerical analyses would be excluded if one additionally had demanded agreement with the cross-section limits resulting from the searches for $e^+e^- \to h_{95} \to \tau^+\tau^-$ at LEP [5] for each parameter point, independently of whether this search was selected as the most sensitive search based on the expected limits following the approach implemented in `HiggsBounds`. Applying the exclusion limits from this experimental search in combination with the application of the exclusion limits of the search that was selected by `HiggsBounds` effectively yields a limit that is stronger than an overall 95% C.L.. In our analysis above we followed the approach to maintain a statistical interpretation of the applied cross-section limits from BSM Higgs-boson searches as an overall exclusion bound at the 95% C.L. and therefore did not impose the limits from the LEP searches in the $\tau^+\tau^-$ final states as additional constraint. However, in order to demonstrate the potential impact of those limits on the parameter space favoured by the excesses at 95 GeV, we show in figure 8 (corresponding to the right plot of figure 1) and figure 9 (corresponding to figure 3) the signal rates of the state h_{95}, where the parameter points that predict a cross section larger than the LEP $\tau\tau$ limit are shown in grey. As explained above, the parameter points shown in figure 8 were obtained based on the condition shown in eq. (4.3), such that the LEP excess in the $h_{95} \to b\bar{b}$ decay mode is not taken into account, whereas the parameter points shown in figure 9 were obtained based on the condition shown in eq. (4.5) that includes the contribution χ^2_{bb}.

JHEP08(2022)201

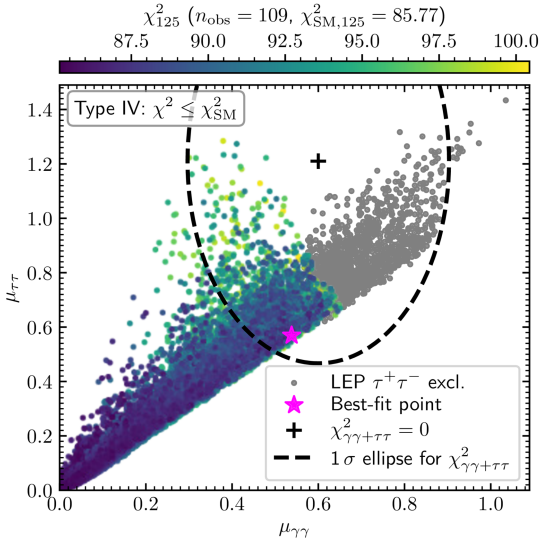

Figure 8. As in the right plot of figure 1, but those parameter points are shown in grey (plotted below the colored points) that would be excluded by the LEP limit in the $\tau^+\tau^-$ final state if that channel had been selected in order to determine the 95% C.L. limit.

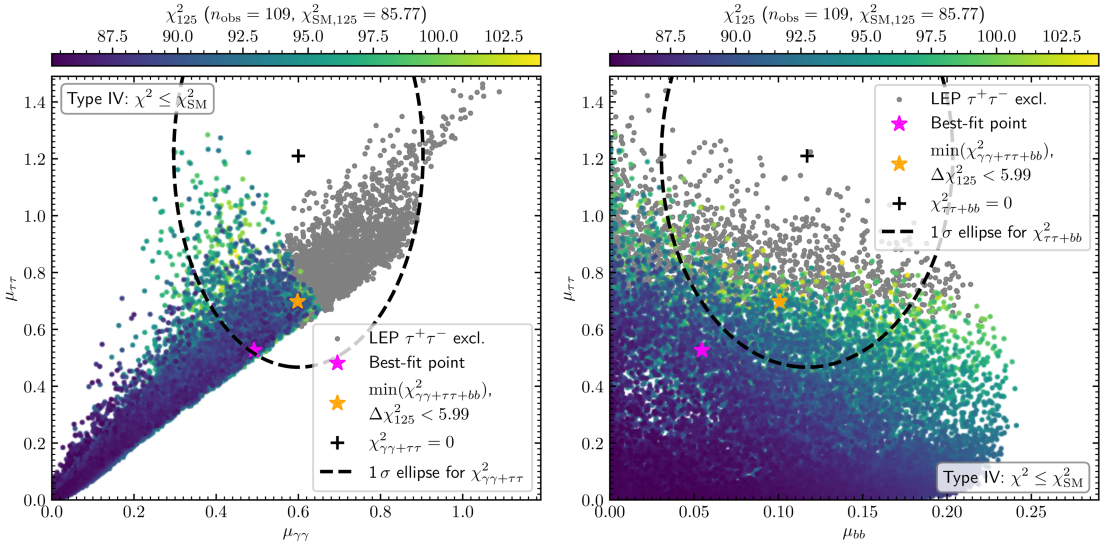

Figure 9. As in figure 3, but those parameter points are shown in grey (plotted below the colored points) that would be excluded by the LEP limit in the $\tau^+\tau^-$ final state if that channel had been selected in order to determine the 95% C.L. limit.

JHEP08(2022)201

References

[1] ATLAS collaboration, *Observation of a new particle in the search for the Standard Model Higgs boson with the ATLAS detector at the LHC*, *Phys. Lett. B* **716** (2012) 1 [arXiv:1207.7214] [INSPIRE].

[2] CMS collaboration, *Observation of a New Boson at a Mass of 125 GeV with the CMS Experiment at the LHC*, *Phys. Lett. B* **716** (2012) 30 [arXiv:1207.7235] [INSPIRE].

[3] ATLAS and CMS collaborations, *Measurements of the Higgs boson production and decay rates and constraints on its couplings from a combined ATLAS and CMS analysis of the LHC pp collision data at $\sqrt{s} = 7$ and 8 TeV*, *JHEP* **08** (2016) 045 [arXiv:1606.02266] [INSPIRE].

[4] OPAL collaboration, *Decay mode independent searches for new scalar bosons with the OPAL detector at LEP*, *Eur. Phys. J. C* **27** (2003) 311 [hep-ex/0206022] [INSPIRE].

[5] LEP Working Group for Higgs boson searches, ALEPH, DELPHI, L3 and OPAL collaborations, *Search for the standard model Higgs boson at LEP*, *Phys. Lett. B* **565** (2003) 61 [hep-ex/0306033] [INSPIRE].

[6] ALEPH, DELPHI, L3, OPAL and LEP Working Group for Higgs Boson Searches collaborations, *Search for neutral MSSM Higgs bosons at LEP*, *Eur. Phys. J. C* **47** (2006) 547 [hep-ex/0602042] [INSPIRE].

[7] CDF and D0 collaborations, *Updated Combination of CDF and D0 Searches for Standard Model Higgs Boson Production with up to 10.0 fb^{-1} of Data*, (2012) [arXiv:1207.0449] [INSPIRE].

[8] CMS collaboration, *Search for new resonances in the diphoton final state in the mass range between 70 and 110 GeV in pp collisions at $\sqrt{s} = 8$ and 13 TeV*, Tech. Rep., CERN, Geneva (2017).

[9] CMS collaboration, *Search for a standard model-like Higgs boson in the mass range between 70 and 110 GeV in the diphoton final state in proton-proton collisions at $\sqrt{s} = 8$ and 13 TeV*, *Phys. Lett. B* **793** (2019) 320 [arXiv:1811.08459] [INSPIRE].

[10] CMS collaboration, *Search for additional neutral MSSM Higgs bosons in the $\tau\tau$ final state in proton-proton collisions at $\sqrt{s} = 13$ TeV*, *JHEP* **09** (2018) 007 [arXiv:1803.06553] [INSPIRE].

[11] ATLAS collaboration, *Search for resonances in the 65 to 110 GeV diphoton invariant mass range using 80 fb^{-1} of pp collisions collected at $\sqrt{s} = 13$ TeV with the ATLAS detector*, Tech. Rep., CERN, Geneva (2018).

[12] CMS collaboration, *Searches for additional Higgs bosons and vector leptoquarks in $\tau\tau$ final states in proton-proton collisions at $\sqrt{s} = 13$ TeV*, Tech. Rep., CERN, Geneva (2022).

[13] CMS collaboration, *Search for new resonances in the diphoton final state in the mass range between 80 and 110 GeV in pp collisions at $\sqrt{s} = 8$ TeV*, Tech. Rep., CERN, Geneva (2015).

[14] S. Heinemeyer and T. Stefaniak, *A Higgs Boson at 96 GeV?!*, *PoS* **CHARGED2018** (2019) 016 [arXiv:1812.05864] [INSPIRE].

[15] J. Cao, X. Guo, Y. He, P. Wu and Y. Zhang, *Diphoton signal of the light Higgs boson in natural NMSSM*, *Phys. Rev. D* **95** (2017) 116001 [arXiv:1612.08522] [INSPIRE].

[16] A. Azatov, R. Contino and J. Galloway, *Model-Independent Bounds on a Light Higgs*, *JHEP* **04** (2012) 127 [*Erratum ibid.* **04** (2013) 140] [arXiv:1202.3415] [INSPIRE].

JHEP08(2022)201

[17] S. Heinemeyer, *A Higgs boson below 125 GeV?!*, *Int. J. Mod. Phys. A* **33** (2018) 1844006 [INSPIRE].

[18] F. Richard, *Indications for extra scalars at LHC? — BSM physics at future e^+e^- colliders*, arXiv:2001.04770 [INSPIRE].

[19] P.J. Fox and N. Weiner, *Light Signals from a Lighter Higgs*, *JHEP* **08** (2018) 025 [arXiv:1710.07649] [INSPIRE].

[20] F. Richard, *Search for a light radion at HL-LHC and ILC250*, arXiv:1712.06410 [INSPIRE].

[21] U. Haisch and A. Malinauskas, *Let there be light from a second light Higgs doublet*, *JHEP* **03** (2018) 135 [arXiv:1712.06599] [INSPIRE].

[22] L. Liu, H. Qiao, K. Wang and J. Zhu, *A Light Scalar in the Minimal Dilaton Model in Light of LHC Constraints*, *Chin. Phys. C* **43** (2019) 023104 [arXiv:1812.00107] [INSPIRE].

[23] T. Biekötter, S. Heinemeyer and C. Muñoz, *Precise prediction for the Higgs-boson masses in the $\mu\nu$ SSM*, *Eur. Phys. J. C* **78** (2018) 504 [arXiv:1712.07475] [INSPIRE].

[24] T. Biekötter, S. Heinemeyer and C. Muñoz, *Precise prediction for the Higgs-Boson Masses in the $\mu\nu$SSM with three right-handed neutrino superfields*, *Eur. Phys. J. C* **79** (2019) 667 [arXiv:1906.06173] [INSPIRE].

[25] D. Liu, J. Liu, C.E.M. Wagner and X.-P. Wang, *A Light Higgs at the LHC and the B-Anomalies*, *JHEP* **06** (2018) 150 [arXiv:1805.01476] [INSPIRE].

[26] J.A. Aguilar-Saavedra and F.R. Joaquim, *Multiphoton signals of a (96 GeV?) stealth boson*, *Eur. Phys. J. C* **80** (2020) 403 [arXiv:2002.07697] [INSPIRE].

[27] F. Domingo, S. Heinemeyer, S. Paßehr and G. Weiglein, *Decays of the neutral Higgs bosons into SM fermions and gauge bosons in the $\mathcal{CP}$-violating NMSSM*, *Eur. Phys. J. C* **78** (2018) 942 [arXiv:1807.06322] [INSPIRE].

[28] K. Choi, S.H. Im, K.S. Jeong and C.B. Park, *Light Higgs bosons in the general NMSSM*, *Eur. Phys. J. C* **79** (2019) 956 [arXiv:1906.03389] [INSPIRE].

[29] W.G. Hollik, S. Liebler, G. Moortgat-Pick, S. Paßehr and G. Weiglein, *Phenomenology of the inflation-inspired NMSSM at the electroweak scale*, *Eur. Phys. J. C* **79** (2019) 75 [arXiv:1809.07371] [INSPIRE].

[30] J. Cao, X. Jia, Y. Yue, H. Zhou and P. Zhu, *96 GeV diphoton excess in seesaw extensions of the natural NMSSM*, *Phys. Rev. D* **101** (2020) 055008 [arXiv:1908.07206] [INSPIRE].

[31] T. Biekötter, M. Chakraborti and S. Heinemeyer, *A 96 GeV Higgs boson in the N2HDM*, *Eur. Phys. J. C* **80** (2020) 2 [arXiv:1903.11661] [INSPIRE].

[32] C.-Y. Chen, M. Freid and M. Sher, *Next-to-minimal two Higgs doublet model*, *Phys. Rev. D* **89** (2014) 075009 [arXiv:1312.3949] [INSPIRE].

[33] M. Mühlleitner, M.O.P. Sampaio, R. Santos and J. Wittbrodt, *The N2HDM under Theoretical and Experimental Scrutiny*, *JHEP* **03** (2017) 094 [arXiv:1612.01309] [INSPIRE].

[34] T. Biekötter, M. Chakraborti and S. Heinemeyer, *An N2HDM Solution for the possible 96 GeV Excess*, *PoS* **CORFU2018** (2019) 015 [arXiv:1905.03280] [INSPIRE].

[35] T. Biekötter, M. Chakraborti and S. Heinemeyer, *The "96 GeV excess" in the N2HDM*, in *31st Rencontres de Blois on Particle Physics and Cosmology*, (2019) [arXiv:1910.06858] [INSPIRE].

JHEP08(2022)201

[36] T. Biekötter, M. Chakraborti and S. Heinemeyer, *The "96 GeV excess" at the ILC*, in *International Workshop on Future Linear Colliders*, (2020) [arXiv:2002.06904] [INSPIRE].

[37] T. Biekötter, M. Chakraborti and S. Heinemeyer, *The "96 GeV excess" at the LHC*, *Int. J. Mod. Phys. A* **36** (2021) 2142018 [arXiv:2003.05422] [INSPIRE].

[38] S. Heinemeyer, C. Li, F. Lika, G. Moortgat-Pick and S. Paasch, *A 96 GeV Higgs Boson in the 2HDM plus Singlet*, arXiv:2112.11958 [INSPIRE].

[39] T. Biekötter, A. Grohsjean, S. Heinemeyer, C. Schwanenberger and G. Weiglein, *Possible indications for new Higgs bosons in the reach of the LHC: N2HDM and NMSSM interpretations*, *Eur. Phys. J. C* **82** (2022) 178 [arXiv:2109.01128] [INSPIRE].

[40] T. Biekötter and M.O. Olea-Romacho, *Reconciling Higgs physics and pseudo-Nambu-Goldstone dark matter in the S2HDM using a genetic algorithm*, *JHEP* **10** (2021) 215 [arXiv:2108.10864] [INSPIRE].

[41] R. Coimbra, M.O.P. Sampaio and R. Santos, *ScannerS: Constraining the phase diagram of a complex scalar singlet at the LHC*, *Eur. Phys. J. C* **73** (2013) 2428 [arXiv:1301.2599] [INSPIRE].

[42] M. Mühlleitner, M.O.P. Sampaio, R. Santos and J. Wittbrodt, *ScannerS: parameter scans in extended scalar sectors*, *Eur. Phys. J. C* **82** (2022) 198 [arXiv:2007.02985] [INSPIRE].

[43] K.G. Klimenko, *On Necessary and Sufficient Conditions for Some Higgs Potentials to Be Bounded From Below*, *Theor. Math. Phys.* **62** (1985) 58 [INSPIRE].

[44] W.G. Hollik, G. Weiglein and J. Wittbrodt, *Impact of Vacuum Stability Constraints on the Phenomenology of Supersymmetric Models*, *JHEP* **03** (2019) 109 [arXiv:1812.04644] [INSPIRE].

[45] https://gitlab.com/jonaswittbrodt/EVADE.

[46] P.M. Ferreira, M. Mühlleitner, R. Santos, G. Weiglein and J. Wittbrodt, *Vacuum Instabilities in the N2HDM*, *JHEP* **09** (2019) 006 [arXiv:1905.10234] [INSPIRE].

[47] P. Bechtle, S. Heinemeyer, O. Stål, T. Stefaniak and G. Weiglein, *HiggsSignals: Confronting arbitrary Higgs sectors with measurements at the Tevatron and the LHC*, *Eur. Phys. J. C* **74** (2014) 2711 [arXiv:1305.1933] [INSPIRE].

[48] O. Stål and T. Stefaniak, *Constraining extended Higgs sectors with HiggsSignals*, *PoS* **EPS-HEP2013** (2013) 314 [arXiv:1310.4039] [INSPIRE].

[49] P. Bechtle, S. Heinemeyer, O. Stål, T. Stefaniak and G. Weiglein, *Probing the Standard Model with Higgs signal rates from the Tevatron, the LHC and a future ILC*, *JHEP* **11** (2014) 039 [arXiv:1403.1582] [INSPIRE].

[50] P. Bechtle, S. Heinemeyer, T. Klingl, T. Stefaniak, G. Weiglein and J. Wittbrodt, *HiggsSignals-2: Probing new physics with precision Higgs measurements in the LHC 13 TeV era*, *Eur. Phys. J. C* **81** (2021) 145 [arXiv:2012.09197] [INSPIRE].

[51] P. Bechtle, O. Brein, S. Heinemeyer, G. Weiglein and K.E. Williams, *HiggsBounds: Confronting Arbitrary Higgs Sectors with Exclusion Bounds from LEP and the Tevatron*, *Comput. Phys. Commun.* **181** (2010) 138 [arXiv:0811.4169] [INSPIRE].

[52] P. Bechtle, O. Brein, S. Heinemeyer, G. Weiglein and K.E. Williams, *HiggsBounds 2.0.0: Confronting Neutral and Charged Higgs Sector Predictions with Exclusion Bounds from LEP and the Tevatron*, *Comput. Phys. Commun.* **182** (2011) 2605 [arXiv:1102.1898] [INSPIRE].

JHEP08(2022)201

[53] P. Bechtle et al., *Recent Developments in HiggsBounds and a Preview of HiggsSignals*, *PoS* **CHARGED2012** (2012) 024 [arXiv:1301.2345] [INSPIRE].

[54] P. Bechtle et al., HiggsBounds – 4*: Improved Tests of Extended Higgs Sectors against Exclusion Bounds from LEP, the Tevatron and the LHC*, *Eur. Phys. J. C* **74** (2014) 2693 [arXiv:1311.0055] [INSPIRE].

[55] P. Bechtle, S. Heinemeyer, O. Stål, T. Stefaniak and G. Weiglein, *Applying Exclusion Likelihoods from LHC Searches to Extended Higgs Sectors*, *Eur. Phys. J. C* **75** (2015) 421 [arXiv:1507.06706] [INSPIRE].

[56] P. Bechtle et al., *HiggsBounds-5: Testing Higgs Sectors in the LHC 13 TeV Era*, *Eur. Phys. J. C* **80** (2020) 1211 [arXiv:2006.06007] [INSPIRE].

[57] ATLAS collaboration, *Search for charged Higgs bosons decaying into a top-quark and a bottom-quark at* $\sqrt{s} = 13$ *TeV with the ATLAS detector*, Tech. Rep., CERN, Geneva (Aug, 2020).

[58] ATLAS collaboration, *Search for heavy Higgs bosons decaying into two tau leptons with the ATLAS detector using pp collisions at* $\sqrt{s} = 13$ *TeV*, *Phys. Rev. Lett.* **125** (2020) 051801 [arXiv:2002.12223] [INSPIRE].

[59] J. Haller, A. Hoecker, R. Kogler, K. Mönig, T. Peiffer and J. Stelzer, *Update of the global electroweak fit and constraints on two-Higgs-doublet models*, *Eur. Phys. J. C* **78** (2018) 675 [arXiv:1803.01853] [INSPIRE].

[60] M.E. Peskin and T. Takeuchi, *A new constraint on a strongly interacting Higgs sector*, *Phys. Rev. Lett.* **65** (1990) 964 [INSPIRE].

[61] M.E. Peskin and T. Takeuchi, *Estimation of oblique electroweak corrections*, *Phys. Rev. D* **46** (1992) 381 [INSPIRE].

[62] W. Grimus, L. Lavoura, O.M. Ogreid and P. Osland, *The oblique parameters in multi-Higgs-doublet models*, *Nucl. Phys. B* **801** (2008) 81 [arXiv:0802.4353] [INSPIRE].

[63] G. Funk, D. O'Neil and R.M. Winters, *What the Oblique Parameters S, T, and U and Their Extensions Reveal About the 2HDM: A Numerical Analysis*, *Int. J. Mod. Phys. A* **27** (2012) 1250021 [arXiv:1110.3812] [INSPIRE].

[64] R.V. Harlander, S. Liebler and H. Mantler, *SusHi: A program for the calculation of Higgs production in gluon fusion and bottom-quark annihilation in the Standard Model and the MSSM*, *Comput. Phys. Commun.* **184** (2013) 1605 [arXiv:1212.3249] [INSPIRE].

[65] R.V. Harlander, S. Liebler and H. Mantler, *SusHi Bento: Beyond NNLO and the heavy-top limit*, *Comput. Phys. Commun.* **212** (2017) 239 [arXiv:1605.03190] [INSPIRE].

[66] A. Djouadi, J. Kalinowski and M. Spira, *HDECAY: A Program for Higgs boson decays in the standard model and its supersymmetric extension*, *Comput. Phys. Commun.* **108** (1998) 56 [hep-ph/9704448] [INSPIRE].

[67] J.M. Butterworth et al., *THE TOOLS AND Monte Carlo WORKING GROUP Summary Report from the Les Houches 2009 Workshop on TeV Colliders*, in *6th Les Houches Workshop on Physics at TeV Colliders*, (2010) [arXiv:1003.1643] [INSPIRE].

[68] A. Djouadi, J. Kalinowski, M. Muehlleitner and M. Spira, *HDECAY: Twenty*$_{++}$ *years after*, *Comput. Phys. Commun.* **238** (2019) 214 [arXiv:1801.09506] [INSPIRE].

JHEP08(2022)201

[69] I. Engeln, M. Mühlleitner and J. Wittbrodt, *N2HDECAY: Higgs Boson Decays in the Different Phases of the N2HDM*, *Comput. Phys. Commun.* **234** (2019) 256 [arXiv:1805.00966] [INSPIRE].

[70] CMS collaboration, *Search for neutral resonances decaying into a Z boson and a pair of b jets or τ leptons*, *Phys. Lett. B* **759** (2016) 369 [arXiv:1603.02991] [INSPIRE].

[71] ATLAS collaboration, *Search for heavy resonances decaying into a W or Z boson and a Higgs boson in final states with leptons and b-jets in 36 fb^{-1} of $\sqrt{s} = 13$ TeV pp collisions with the ATLAS detector*, *JHEP* **03** (2018) 174 [*Erratum ibid.* **11** (2018) 051] [arXiv:1712.06518] [INSPIRE].

[72] ATLAS collaboration, *Search for a heavy Higgs boson decaying into a Z boson and another heavy Higgs boson in the $\ell\ell bb$ final state in pp collisions at $\sqrt{s} = 13$ TeV with the ATLAS detector*, *Phys. Lett. B* **783** (2018) 392 [arXiv:1804.01126] [INSPIRE].

[73] CMS collaboration, *Search for new neutral Higgs bosons through the $H \to ZA \to \ell^+\ell^- b\bar{b}$ process in pp collisions at $\sqrt{s} = 13$ TeV*, *JHEP* **03** (2020) 055 [arXiv:1911.03781] [INSPIRE].

[74] CMS collaboration, *Search for a heavy pseudoscalar boson decaying to a Z and a Higgs boson at $\sqrt{s} = 13$ TeV*, *Eur. Phys. J. C* **79** (2019) 564 [arXiv:1903.00941] [INSPIRE].

[75] ATLAS collaboration, *Search for heavy resonances decaying into a Z boson and a Higgs boson in final states with leptons and b-jets in 139 fb^{-1} of pp collisions at $\sqrt{s} = 13$TeV with the ATLAS detector*, Tech. Rep., CERN, Geneva (Aug, 2020).

[76] CMS collaboration, *Search for a heavy Higgs boson decaying into two lighter Higgs bosons in the $\tau\tau bb$ final state at 13 TeV*, *JHEP* **11** (2021) 057 [arXiv:2106.10361] [INSPIRE].

[77] ATLAS collaboration, *Combined measurements of Higgs boson production and decay using up to 80 fb^{-1} of proton-proton collision data at $\sqrt{s} = 13$ TeV collected with the ATLAS experiment*, *Phys. Rev. D* **101** (2020) 012002 [arXiv:1909.02845] [INSPIRE].

[78] CMS collaboration, *Combined Higgs boson production and decay measurements with up to 137fb-1 of proton-proton collision data at sqrts = 13 TeV*, Tech. Rep., CERN, Geneva (2020).

[79] M. Cepeda et al., *Report from Working Group 2*: Higgs Physics at the HL-LHC and HE-LHC, *CERN Yellow Rep. Monogr.* **7** (2019) 221 [arXiv:1902.00134] [INSPIRE].

[80] P. Bambade et al., *The International Linear Collider: A Global Project*, arXiv:1903.01629 [INSPIRE].

[81] CMS collaboration, *Search for heavy Higgs bosons decaying to a top quark pair in proton-proton collisions at $\sqrt{s} = 13$ TeV*, *JHEP* **04** (2020) 171 [arXiv:1908.01115] [INSPIRE].

[82] ATLAS collaboration, *Combination of searches for heavy resonances decaying into bosonic and leptonic final states using 36 fb^{-1} of proton-proton collision data at $\sqrt{s} = 13$ TeV with the ATLAS detector*, *Phys. Rev. D* **98** (2018) 052008 [arXiv:1808.02380] [INSPIRE].

[83] CMS collaboration, *Search for a new scalar resonance decaying to a pair of Z bosons in proton-proton collisions at $\sqrt{s} = 13$ TeV*, *JHEP* **06** (2018) 127 [*Erratum ibid.* **03** (2019) 128] [arXiv:1804.01939] [INSPIRE].

[84] T. Biekötter, S. Heinemeyer, J.M. No, M.O. Olea and G. Weiglein, *Fate of electroweak symmetry in the early Universe: Non-restoration and trapped vacua in the N2HDM*, *JCAP* **06** (2021) 018 [arXiv:2103.12707] [INSPIRE].

JHEP08(2022)201

[85] ATLAS collaboration, *Search for pair production of Higgs bosons in the $b\bar{b}b\bar{b}$ final state using proton-proton collisions at $\sqrt{s} = 13$ TeV with the ATLAS detector*, *JHEP* **01** (2019) 030 [arXiv:1804.06174] [INSPIRE].

[86] ATLAS collaboration, *Combination of searches for Higgs boson pairs in pp collisions at $\sqrt{s} = 13$ TeV with the ATLAS detector*, *Phys. Lett. B* **800** (2020) 135103 [arXiv:1906.02025] [INSPIRE].

[87] ATLAS collaboration, *Search for Higgs boson pair production in the $\gamma\gamma b\bar{b}$ final state with 13 TeV pp collision data collected by the ATLAS experiment*, *JHEP* **11** (2018) 040 [arXiv:1807.04873] [INSPIRE].

JHEP08(2022)201